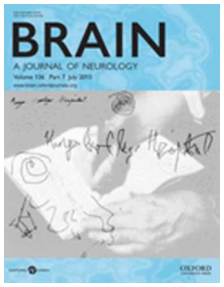

A mitochondrial origin for frontotemporal dementia and amyotrophic lateral sclerosis through *CHCHD10* involvement

Journal:	*Brain*
Manuscript ID:	BRAIN-2014-00021.R1
Manuscript Type:	Original Article
Date Submitted by the Author:	n/a
Complete List of Authors:	Bannwarth, Sylvie; Faculté de Médecine, IRCAN, CNRS UMR 7284/Inserm U1081/UNS; CHU de Nice, Service de Génétique Médicale, Hôpital Archet 2 Ait-El-Mkadem, Samira; Faculté de Médecine, IRCAN, CNRS UMR 7284/Inserm U1081/UNS; CHU de Nice, Service de Génétique Médicale, Hôpital Archet 2 Chaussenot, Annabelle; CHU de Nice, Service de Génétique Médicale, Hôpital Archet 2; Faculté de Médecine, IRCAN, CNRS UMR 7284/Inserm U1081/UNS Genin, Emmanuelle; Faculté de Médecine, IRCAN, CNRS UMR 7284/Inserm U1081/UNS Lacas-Gervais, Sandra; Nice Sophia-Antipolis University, Joint Center for Applied Electron Microscopy Fragaki, Konstantina; Faculté de Médecine, IRCAN, CNRS UMR 7284/Inserm U1081/UNS; CHU de Nice, Service de Génétique Médicale, Hôpital Archet 2 Berg-Alonso, Laetitia; Faculté de Médecine, IRCAN, CNRS UMR 7284/Inserm U1081/UNS Kageyama, Yusuke; Johns Hopkins University School of Medicine, Dpt of Cell Biology Serre, Valérie; UMR7592 CNRS, Jacques Monod Institute, Paris Diderot University Moore, David; Institute of Genetic Medicine, International Centre for Life, Wellcome Trust Centre for Mitochondrial Research VERSCHUEREN, Annie; Timone Hospital, Marseille Teaching Hospital, Department of Neurology Rouzier, Cécile; CHU de Nice, Service de Génétique Médicale, Hôpital Archet 2; Faculté de Médecine, IRCAN, CNRS UMR 7284/Inserm U1081/UNS Le Ber, Isabelle; CR-ICM UMRS975, Hopital de la Salpêtrière; Centre de référence des démences rares, Hopital de la Salpêtrière Augé, Gaelle; CHU de Nice, Service de Génétique Médicale, Hôpital Archet 2; Faculté de Médecine, IRCAN, CNRS UMR 7284/Inserm U1081/UNS

	Cochaud, Charlotte; CHU de Nice, Service de Génétique Médicale, Hôpital Archet 2 Lespinasse, Françoise; Faculté de Médecine, IRCAN, CNRS UMR 7284/Inserm U1081/UNS N'Guyen, Karine; La Timone Hospital, Department of Genetics de Septenville, Anne; Sorbonne université, INSERM U1127, CNRS UMR7225 Brice, Alexis; INSERM U679, Hôpital Pitié-Salpêtrière; Département de Génétique, Cytogénétique et Embryologie, Hôpital Pitié-Salpêtrière Yu-Wai-Man, Patrick; Newcastle University, Wellcome Trust Centre for Mitochondrial Research. Sesaki, Hiromi; Dpt of cell biology, Johns hopkins university school of medicine Pouget, Jean; Hôpital La Timone, Service d'Anatomie Pathologique et de Neuropathologie Paquis-Flucklinger, Véronique; Faculté de Médecine, IRCAN, CNRS UMR 7284/Inserm U1081/UNS; CHU de Nice, Service de Génétique Médicale, Hôpital Archet 2
Key Words:	
Please choose up to 5 keywords from the list:	CHCHD10, ALS, frototemporal dementia, mitochondrial diseases, mutation
Subject category:	Genetics

SCHOLARONE™
Manuscripts
For Review

A mitochondrial origin for frontotemporal dementia and amyotrophic lateral sclerosis through *CHCHD10* involvement

*Sylvie Bannwarth,[1,2] *Samira Ait-El-Mkadem,[1,2] Annabelle Chaussenot,[1,2] Emmanuelle C. Genin,[1] Sandra Lacas-Gervais,[3] Konstantina Fragaki,[1,2] Laetitia Berg-Alonso,[1] Yusuke Kageyama,[4] Valérie Serre,[5] David G. Moore,[6] Annie Verschueren,[7] Cécile Rouzier,[1,2] Isabelle Le Ber,[8,9] Gaëlle Augé,[1,2] Charlotte Cochaud,[2] Françoise Lespinasse,[1] Karine N'Guyen,[10] Anne de Septenville,[8] Alexis Brice,[8] Patrick Yu Wai Man,[6] Hiromi Sesaki,[4] Jean Pouget,[7] Véronique Paquis-Flucklinger[1,2]

* These authors contributed equally to the study

[1]IRCAN, UMR CNRS 7284/INSERM U1081/UNS, School of Medicine, Nice Sophia-Antipolis University, France
[2]Department of Medical Genetics, National Centre for Mitochondrial Diseases, Nice Teaching Hospital, France
[3]Joint Center for Applied Electron Microscopy, Nice Sophia-Antipolis University, France
[4]Department of Cell Biology, Johns Hopkins University School of Medicine, Baltimore, MD, 21205, USA
[5]UMR7592 CNRS, Jacques Monod Institute, Paris Diderot University, France
[6]Wellcome Trust Centre for Mitochondrial Research, Institute of Genetic Medicine, International Centre for Life, Newcastle University, Newcastle upon Tyne NE1 3BZ, UK
[7]Department of Neurology, Timone Hospital, Marseille Teaching Hospital, France
[8]Sorbonne Université, UPMC Univ Paris 06, UM75, Inserm U1127, Cnrs UMR7225, Institut du Cerveau et de la Moelle épinière (ICM), F-75013 Paris, France.
[9]National Reference Centre on Rare Dementias, AP-HP, Groupe Hospitalier Pitié-Salpêtrière, Paris, France
[10]Department of Medical Genetics, Timone Hospital, Marseille Teaching Hospital, France
[11]Newcastle Eye Centre, Royal Victoria Infirmary, Newcastle upon Tyne, NE1 4LP, UK

Running title: *CHCHD10* and mitochondrial disorder

Key words: *CHCHD10*, mitochondrial DNA instability, mitochondrial disorder, FTD-ALS

Word count : 5886 words

Correspondence to:

Prof. Véronique Paquis-Flucklinger
IRCAN UMR CNRS 7284 / INSERM U1081 / UNS
School of Medicine, 28 av de Valombrose,
06107 Nice cedex 2, France.
Tel: (33) 4 93 37 77 86
Fax: (33) 4 93 37 70 33
e-mail: paquis@hermes.unice.fr

For Peer Review

ABSTRACT

Mitochondrial DNA (mtDNA) instability disorders are responsible for a large clinical spectrum, among which amyotrophic lateral sclerosis-like symptoms and frontotemporal dementia are extremely rare. We report a large family with a late-onset phenotype including motor neuron disease, cognitive decline looking like frontotemporal dementia, cerebellar ataxia and myopathy. In all patients, muscle biopsy showed ragged-red and COX negative fibres with combined respiratory chain deficiency and abnormal assembly of complex V. The multiple mtDNA deletions found in skeletal muscle revealed a mtDNA instability disorder. Patient fibroblasts present with respiratory chain deficiency, mitochondrial ultrastructural alterations and fragmentation of the mitochondrial network. Interestingly, expression of matrix-targeted photoactivable GFP showed that mitochondrial fusion was not inhibited in patient fibroblasts. By whole-exome sequencing (WES), we identified a missense mutation (c.176C>T; p.Ser59Leu) in the *CHCHD10* gene that encodes a coiled-coil helix coiled-coil helix protein, whose function is unknown. We show that CHCHD10 is a mitochondrial protein located in the intermembrane space and enriched at cristae junctions. Overexpression of *CHCHD10* mutant allele in HeLa cells led to fragmentation of the mitochondrial network and ultrastructural major abnormalities including loss, disorganization and dilatation of cristae.

The observation of a frontotemporal dementia-amyotrophic lateral sclerosis (FTD-ALS) phenotype in a mitochondrial disease led us to analyse *CHCHD10* in a cohort of 21 families with pathologically proven FTD-ALS. We identified the same missense p.Ser59Leu mutation in one of these FTD-ALS families. This work opens a novel field to explore the pathogenesis of FTD-ALS clinical spectrum by showing that mitochondrial disease may be at the origin of some of these phenotypes.

For Peer Review

INTRODUCTION

Mitochondrial disorders can result from defects in mitochondrial DNA (mtDNA) or in nuclear genes that encode proteins that are imported in the mitochondria. Last years, a growing list of genes responsible for mtDNA instability has been reported (Copeland, 2012; Ylikallio *et al.,* 2012; Shapira *et al.,* 2012). Mutations in these genes lead either to mitochondrial DNA depletion syndrome (MDS), a devastating mitochondrial disease of childhood associated with a significant reduction of mtDNA copy number, or disorders characterized by accumulation of multiple mtDNA deletions in postmitotic tissues (Suomalainen *et al.,* 2010; Copeland, 2012). Diseases associated with deletions comprise commonly known clinical presentations including progressive external ophtalmoplegia (PEO) and ataxia neuropathy syndromes but also some rares disorders (for review see Copeland, 2012). To date, nuclear genes responsible for mtDNA instability disorders mainly fall into three categories : (i) genes encoding proteins directly involved in mtDNA replication, such as *POLG*, *POLG2* or *TWINKLE*, (ii) genes encoding proteins responsible for the maintenance of mitochondrial nucleotide pool, such as *TP, TK2, DGUOK*… and, (iii) genes encoding membrane proteins involved in mitochondrial dynamics, such as *OPA1* or *MFN2* (Amati-Bonneau *et al.,* 2008; Hudson *et al.,* 2008; Rouzier *et al.,* 2012). This third category was recently individualized. Autosomal dominant optic atrophy (ADOA) is mainly related to mutations in the optic atrophy 1 gene (*OPA1*) which encodes a dynamin-like GTPase involved in the fusion of the inner mitochondrial membrane (Delettre *et al.,* 2000). Mitofusin 2 (Mfn2) is one of the two mitofusin proteins also required for mitochondrial fusion. Mfn1 and Mfn2 are conserved integral outer mitochondrial membrane proteins, each consisting of a large GTPase domain and 2 heptad repeat (HR), or putative coil-coiled domains, all of which face the cytoplasm (Koshiba *et al.,* 2004; Meeusen *et al.,* 2004; Song *et al.,* 2009). *MFN2* mutations are a major cause of primary axonal Charcot-Marie-Tooth

For Peer Review

disease type 2A (CMT2A) (Zuchner *et al.,* 2004), an autosomal dominant neuropathy that impairs motor and sensory neurons with the longest axons resulting in earliest symptoms in distal extremities. A subset of *OPA1* missense mutations have been associated with the "ADOA plus" syndrome and with accumulation of mtDNA deletions in muscle (Amati-Bonneau *et al.,* 2008; Hudson *et al.,* 2008). Complex phenotypes have also been associated with *MFN2* mutations. Recently, we reported a large family with optic atrophy beginning in early childhood, associated with axonal neuropathy and mitochondrial myopathy with mtDNA deletions in adult life. The clinical presentation looks like the "ADOA plus" phenotype linked to *OPA1* mutations but is associated with a novel *MFN2* missense mutation, thus confirming the link between mtDNA stability and mitochondrial fusion (Rouzier *et al.,* 2012).

Here, we report the involvement of a novel gene responsible for "mitochondrial DNA breakage" syndrome and frontotemporal lobe dementia-amyotrophic lateral sclerosis (FTD-ALS) through 2 families from French and Spanish origin. The responsible gene, *CHCHD10,* encodes a coiled-coil helix coiled-coil helix protein whose function is unknown. However, CHCHD10 belongs to a family of mitochondrial proteins located in the intermembrane space, some of which interact with OPA1 and are involved in cristae integrity and mitochondrial fusion (Darshi *et al.,* 2011; An *et al., 2012*).

PATIENTS AND METHODS

Patients

The pedigree of the first family of French origin is shown in Fig. 1. All clinical data are summarized in table 1. Blood and tissue samples were obtained after patients had given informed consent. The index case was a 67-year-old woman (IV-6), who developed a cerebellar ataxia at 50 years of age, associated with progressive bulbar syndrome, dementia

For Peer Review

and sensorineural deafness. Clinical examination showed cerebellar ataxia, Babinski sign, areflexia and bulbar palsy with dysarthria and dysphagia. Neuropsychological tests revealed a frontal lobe syndrome. Laboratory investigations showed normal lactate concentrations (1.6 mmol/l, normal <2.1 mmol /l). She died at 67 years of age.

The age of onset of the 7 other patients who underwent a muscle biopsy was between 49 and 65 year-old. Three patients presented a motor neuron disease (MND), 2 a cerebellar ataxia and the last two had a MND and a cerebellar ataxia, like the index case. All developed cognitive disorders with mainly a frontal lobe syndrome, except patient V-2 who died at 51 year-old. Neuropsychological evaluation of patient IV-3 showed severe impairment in episodic memory, attention, verbal fluency and executive functions with behavioral changes corresponding to frontal dementia. Brain MRI of patient V-10 was normal and the one of the patient IV-3 showed moderate cortical atrophy. Brain MRI performed in 4 other patients (III-2, IV-11, IV-13, V-2) showed no specific abnormality. Proximal weakness was observed in 4 individuals (IV-3, IV-11, IV-13 and IV-15) with bilateral ptosis and facial paresis in patient IV-15. Electromyography excluded peripheral neuropathy with normal test (V-10), chronic neurogenic changes suggesting a lower motor neuron disease (IV-15) or myopathic abnormalities only (IV-3). Patients IV-3 and V-10 are still alive, all others died after more than 10 years of evolution.

Other affected individuals had no muscle biopsy (I-1, II-1, II-2, II-6, III-1, III-4, III-5, III-6, III-7, III-8 and IV-9). They presented dementia, progressive bulbar syndrome with dysarthria and dysphagia, and became bedridden.

Muscle histopathology and ultrastructure

Muscle samples were frozen in cooled isopentane and stored in liquid nitrogen for histological and histoenzymatic analysis including Gomori modified trichrome staining, cytochrome *c* oxydase (COX) activity, succinate dehydrogenase (SDH) activity and double

For Peer Review

COX/SDH staining according to standard protocols. A fragment of muscle was also fixed in 2% glutaraldehyde and processed for ultrastructural analysis by electron microscopy.

OXPHOS spectrophotometric measurements

Enzymatic spectrophotometric measurements of the OXPHOS respiratory chain complexes and citrate synthase were performed at 37°C on muscle crude homogenates and fibroblasts according to standard procedures (Rustin *et al.,* 1994).

Polarographic study

Polarographic studies on fibroblasts of intact cell respiration and digitonin (0.004%)-permeabilized cells mitochondrial substrate oxidation were carried out as previously described (Rustin *et al.,* 1994).

Blue native gel electrophoresis (BN-PAGE) and immunoblotting

15 µg of muscle mitochondrial respiratory complexes, obtained by solubilisation in a solution of 1.5 M aminocaproic acid (Sigma-Aldrich), 75 mM BIS-TRIS (Sigma-Aldrich) and 4% dodecyl-β-D-maltoside (Sigma-Aldrich), were separated by BN-PAGE on a 4–13% acrylamide gradient gel (Schägger *et al.,* 2001). Then they were electroblotted onto a PVDF membrane, prior to sequential incubation with specific antibodies directed against GRIM19 subunit of complex I, SDHA subunit of complex II, UQCRC2 subunit of complex III, MTCO1 subunit of complex IV and ATP5A subunit of complex V (Mitosciences) allowing to verify that samples were equally loaded between patients and controls.

Protein measurement

Proteins were measured according to Bradford microassay (Bradford, 1976).

mtDNA molecular analysis

Total DNA was extracted using standard phenol chloroform procedure. Long-range PCR and Southern blot analysis were performed as previously described (Paul *et al.,* 1996; Moraes *et al.,* 1996). mtDNA quantification in muscle was performed by real-time quantitative PCR as

For Peer Review

described by Rouzier *et al*., 2010. Primer sequences and PCR conditions are available on request.

Sequencing of nuclear genes

The coding regions of *POLG* (NM_002693.2), *SLC25A4* (ANT1*)* (NM_001151.3) and *PEO1* (Twinkle*)* (NM_021830.4) genes were sequenced as previously described (Naimi *et al.,* 2006). PCR products were purified with Illustra ExoStar enzyme (GE Healthcare), processed with an ABI PRISM® dRhodamine Terminator Cycle Sequencing Ready Reaction kit (Applied Biosystems) and analyzed on an ABI 3130XL automated sequencer (Applied Biosystems).

Cell culture

Skin punches were obtained from patient V-10 after informed consent. Primary fibroblast cultures were established using standard procedures in RPMI supplemented with 10% Fetal Bovine Serum (FBS), 45µg/ml uridine and 275µg/ml sodium pyruvate. Cultures were incubated at 37°C with 5% CO_2. For galactose conditions, medium was replaced 24h before experiments by glucose-free medium containing 5mM galactose and 5mM pyruvate (Zanna *et al.,* 2008).

HeLa cells were maintained in DMEM supplemented with penicillin (100U/ml)/streptomycin (0.1mg/ml), 10% fetal calf serum (FCS), at 37°C in a humidified atmosphere with 5% CO_2 in air. For transient transfections, HeLa cells were transfected using Lipofectamine 2000 (Invitrogen) according to the manufacturer's instructions.

Mitochondrial network analysis

For mitochondrial staining, cells were incubated in a 100nM solution of MitoTracker red (Invitrogen) for 15 min, medium was replaced by HeLa cells culture medium incubated 2 h at 37°C and washed in PBS. The samples were fixed with paraformaldehyde (PFA) 4% (Electron Microscopy Sciences), washed with PBS, and mounted on glass slides using

For Peer Review

Prolong Gold Antifade Reagent (Molecular Probes). For immunostaining, cells were fixed with 4% PFA, washed five times with PBS and permeabilised with 2% Triton X-100. After PBS washing, coverslips were incubated with 5% BSA (Bovin Serum Albumin) for 30 min at room temperature before adding mouse anti-FlagM2 (Agilent Technologies) (1/2000 antibody diluted with PBS-BSA 5%), mouse anti-HA (Cell Signaling) (1/100 antibody diluted with PBS-BSA 5%) or rabbit anti-FlagM2 (Cell Signaling) (1/800 antibody diluted with PBS-BSA 5%). The samples were incubated at room temperature for 1h, PBS washed, and then incubated with fluorescent secondary antibody goat anti-mouse Alexa 488 (Life Technologies) (1/1000 antibody diluted with PBS-BSA 1%) or antibody goat anti-rabbit Alexa 647 (Life Technologies) (1/1000 antibody diluted with PBS-BSA 1%) for 1 hour at room temperature. The coverslips were washed five times with PBS, mounted on glass slides using Prolong Gold Antifade Reagent (Molecular Probes) and analyzed using a Zeiss LSM510 meta confocal laser-scanning microscope.

The images were deconvolved with Huygens Essential Software™ (Scientific Volume Imaging) using a theoretically calculated point spread function (PSF) for each of the dyes. All selected images were iteratively deconvolved with a maximum iterations scored 40 and a quality threshold at 0.05. The deconvolved images were used for quantitative mitochondrial network analysis with Huygens Essentiel Software™ with the following standardised set of parameters: threshold = 25% and seed = 0% for each cell types and garbage = 5 or 10 for HeLa cells and fibroblasts respectively. The quantitative data were further analysed in Microsoft Excel and GraphPad Prism 5 (GraphPad Software). Mitochondrial network length was quantified for 35 randomly-selected individual cells.

Data are represented as mean ± S.E.M. Statistical analyses were performed by Student's unpaired t-test using GraphPad Prism 5 (GraphPad Software).

For Peer Review

Exome sequencing

Genomic DNA was extracted from blood and 3µg were fragmented by sonication. Exome targets were enriched with the SureSelect Human All Exon v4+UTR – 70 Mb Kit (Agilent technologies) and sequenced on the Illumina HiSEQ 2000 platform (Illumina). Raw image files were processed by the IlluminaReal Time Analysis pipeline for base calling and generating the read sets. The bioinfomatics analysis of sequencing data was based on the Illumina CASAVA pipeline (v1.8). CASAVA performs alignment of the 2x75 bp paired-end sequence reads to the hg19 reference genome, calls the SNPs based on the allele calls and read depth, and detects variants (SNPs &Indels). The alignment algorithm used was ELANDv2e. Only the positions included in the bait coordinates were conserved. The web application ERIS (Integragen) was used for data visualization and prioritization of variants.

For mutation validation and segregation analysis, a part of *CHCHD10* (NM_213720.1) spanning the mutation site in exon 2 was amplified with the following primers: 5'-TCGGGCCAGCCGGGGCTC-3' (forward) and 5'-GGAAGCCTGCCTCTAAGTGA-3' (reverse). Purification and sequencing of PCR products were performed as described above.

Homology modelling of human CHCHD10

Using the threading program PHYRE2 (Kelley *et al.,* 2009), 142 residues of CHCHD10 (Met1 to Pro142) were modeled using CHCHD5 as template (PDB ID: 2LQL). Swiss-Pdb Viewer 3.7 (http://www.expasy.org/spdbv) was used to analyze the structural insight into CHCHD10 mutation and visualize the structure.

Plasmid constructions

The human full-length *CHCHD10* cDNA was amplified by RT-PCR from total RNA of patient fibroblasts by using Transcription First strand cDNA synthesis kit (Roche) and Taq PCRx DNA polymerase (Invitrogen).

For Peer Review

We used the following primers: 5'-GGATCCACCGCCGCCACCATG-3' (forward) and 5'-CTCGAGGGGCAGGGAGCTCAG-3' (reverse) containing *Bam*HI and *Xho*I restriction sites, respectively. Restriction-digested PCR products were cloned into pCMV-3tag-3A to generate Flag-tagged CHCHD10. Sequencing of the clones obtained led to the identification of plasmids coding for wild-type ($CHCHD10^{WT}$) and mutant ($CHCHD10^{S59L}$) cDNAs.

Western blotting

5-25 µg of total protein extracts were separated on acrylamide-SDS gels and transferred to PVDF membranes (Millipore, Saint-Quentin). Specific proteins were detected by using mouse anti-Mfn2 (1/2000, Abcam, #ab56889), anti-VDAC (1/2000, Millipore, #MABN504), anti-Flag M2 (1/2000, Agilent Technologies, #200412), anti-PCNA (1/5000, BD Biosciences, #610664), rabbit polyclonal anti-mitofilin (1/2000; Proteintech #10179-1-AP), anti-GAPDH (1/20000, Abcam #ab9485), anti-β tubulin (1/10000, Sigma-Aldrich, #T4026), anti-SMAC (1/4000, Abcam #ab8114), anti-TOM 20 (1/5000, BD Biosciences, #612278), anti-CHCHD10 (1/500, Sigma-Aldrich #HPA003440) and goat polyclonal anti-Hsp60 (1/4000, Santa Cruz, #sc-1052) antibodies. Anti-mouse, anti-rabbit or anti-goat secondary antibody (Dako) was used at 1/10000 and signals were detected using a chemiluminescence system (Immobilon Western HRP Chemilumiscent substrates, Millipore). Human multiple tissue blot was used as described by the manufacturer (G-Biosciences).

Isolation of mitochondria and mitoplast preparation

Mitochondria were isolated from HeLa transfected cells using Q-Proteome mitochondria isolation kit (Qiagen) as described by the manufacturer. Mitochondria were treated with Proteinase K (Invitrogen) in the presence or absence of 0.2% TritonX-100 exactly as described in Bannwarth *et al.,* 2012. To prepare the mitoplasts, we used a digitonin treatment. Briefly, purified mitochondria were suspended in suspension buffer (250 mM sucrose, 1mM EDTA, 20mM HEPES-NaOH, pH7.4). Mitochondria were treated with digitonin (2mg/ml)

For Peer Review

15 min at room temperature. The resulting mitoplasts were treated 10 min at room temperature with Proteinase K (100ng/µl). Proteolysis was halted by the addition of 10mM PMSF (Sigma-Aldrich) for 15 min on ice. Laemmli sample buffer was added directly to samples, boiled and loaded on SDS-PAGE.

Alkali extraction of intact mitochondria

Alkali extraction was performed as previously described (Bannwarth *et al.,* 2012). Briefly, intact isolated mitochondria (25µg) were treated with 0.1M Na_2CO_3 (pH 11.5) for 30 min on ice, and then centrifuged at 16,000g for 15 min at 4°C. Supernatants were retained and pellets were washed once and then resuspended in an equivalent volume of homogenization buffer (250mM sucrose, 1mM EDTA, 20mM Hepes-NaOH pH7.4, plus protease inhibitor). Equivalent volumes were analyzed by immunoblot.

Immunoelectron microscopy

Cells were fixed with 2% paraformaldehyde, 0.2% glutaraldehyde in 0.1 M phosphate buffer (pH 7.4) for 2 hr and were processed for ultracryomicrotomy according to a slightly modified Tokuyasu method (Tokuyasu, 1973). In brief, cell suspension was spun down in 10% gelatin. After immersion in 2.3 M sucrose (in [pH 7.4], 0.1 M PB) overnight at 4°C, the samples were rapidly frozen in liquid nitrogen. Ultrathin (70 nm thick) cryosections were prepared with an ultracryomicrotome (Leica EMFCS) and mounted on formvar-coated nickel grids (Electron Microscopy Sciences). Immunostainings were processed with an automated immunogold labeling system Leica EM IGL as following: the grids were incubated successively in PBS containing 50 mM NH4Cl (5 min twice), PBS containing 1% BSA (5 min twice), PBS containing rabbit anti-CHCHD10 (Sigma-Aldrich) or anti-Hsp60 (Abcam, #ab46798) antibody in 1% BSA for 1 h, PBS containing 0.1% BSA (5 min 3 times), PBS containing 1% BSA and 10 nm colloidal gold conjugated protein AG (CMC), PBS containing 0.1% BSA for

For Peer Review

5 min, PBS for 5 min twice. Lastly, the samples were fixed for 10 min with 1% glutaraldehyde, rinsed in distilled water and were contrasted with a mixture of 1.8% methylcellulose and 0.3% uranyl acetate on ice. After having been dried in air, sections were examined under a JEOL 1400 transmission electron microscope.

Mitochondrial fusion assay

Mitochondrial fusion was examined using mitochondria-targeted photoactivatable GFP (mitoPAGFP), as described (Karbowski *et al.*, 2004). The matrix-targeted presequence from Su9 (Wakabayashi *et al.*, 2009) was fused to the N-terminus of photoactivatable GFP (Addgene #11910) and cloned into the lentiviral vector pHR-SIN (Kim *et al.*, 2011). Fibroblasts were infected with lentiviral particles carrying mitoPAGFP. 30 min before observation, fibroblasts were stained with 7 nM tetramethylrhodamine ethyl ester to visualize mitochondria. mitoPAGFP was photoactivated by 405-nm light (30% power, three times) in a small region (30 x 30 pixels) using a Zeiss 780 LSM confocal microscope with an environmentally controlled chamber. Images were taken at 15-min intervals for 60 min. Fluorescence intensity of mitoPAGFP was quantified using NIH Image J.

RESULTS

Mitochondrial myopathy with multiple mtDNA deletions in patients

Muscle biopsy was performed in 8 patients after informed consent (III-2, IV-3, IV-6, IV-11, IV-13, IV-15, V-2, V-10) (Fig.1). Muscle analysis of the index case (IV-6) showed typical features of mitochondrial myopathy including intracellular lipid accumulation with COX-negative and ragged-red fibres (RRF) (30%) (Fig.2A-B). Electron microscopy showed altered morphology of mitochondria and cristae organization with paracristalline inclusions (Fig.2C). Similar findings with numerous RRF and COX-deficient fibres were found in all patients tested. Spectrophotometric analysis showed a combined respiratory chain deficiency in most

For Peer Review

patients (Table 1). BN-PAGE assay of patients IV-3 and V-2 revealed smaller bands with antibody against complex V corresponding to assembly defect or increased instability (Fig.2D). All patients carried multiple mtDNA deletions in muscle identified by both long range PCR (not shown) and Southern blot analysis (Fig.2E). The determination of relative mtDNA copy number was performed by real-time quantitative PCR without finding any depletion (not shown).

Respiratory chain deficiency, abnormal mitochondrial network and mitochondrial ultrastructural alterations in patient fibroblasts

Spectrophotometric analysis of fibroblasts from patient V-10 cultivated in glucose medium revealed no respiratory chain deficiency and polarographic analysis showed normal oxygen consumption and mitochondrial substrate oxidation (Table 2A, 2C). In a glucose-free medium containing galactose, cells are forced to rely predominantly on OXPHOS for ATP production because the carbon source feeds the glycolytic pathway with a low efficiency. In galactose medium, spectrophotometric analysis revealed a multiple RC deficiency in patient fibroblasts and polarographic analysis showed a decrease of oxygen consumption, glutamate/malate and succinate (Table 2B, 2D). BN-PAGE analysis of patient fibroblasts revealed no abnormality including complex V (not shown), the activity of which was normal by spectrophotometry. Multiple mtDNA deletions were not observed and the determination of relative mtDNA copy number was performed by real-time quantitative PCR without finding any depletion (not shown).

We also compared the mitochondrial morphology of fibroblasts from patient V-10 with that obtained from control fibroblasts. After staining with Mitotracker and examination by confocal microscopy, control fibroblasts in glucose medium displayed a typical filamentous interconnected network. Patient fibroblasts presented with a fragmentation of the

For Peer Review

mitochondrial network and less connected mitochondria (Fig.3A-B). We obtained the same results in galactose medium (not shown).

We then performed ultrastructural analysis of patient fibroblasts. Typical mitochondria of control cells had numerous, thin, well□defined cristae, running perpendicularly to the mitochondrial longitudinal axis, and with a regular pattern of parallel organization (Fig.3C). They represented 90% of the mitochondrial profiles seen in two independent, genotype-blind, analyses of control cells. In patient cells, they represented 35% of the mitochondrial profiles. Completely disorganized mitochondria with sparse or absent cristae without recognizable parallel orientation were only observed in patient fibroblasts (18%) (Fig.3D). Less disorganized mitochondria represented 47% of the mitochondrial pattern in patient cells and 10% in control cells (Fig.3E).

No mitochondrial fusion defect in patient fibroblasts

The fragmentation of mitochondrial network observed in patient fibroblasts can be of different origins including a fusion deficiency. Furthermore, genes like *MFN2* or *OPA1* involved in mitochondrial fusion are responsible for complex neurological phenotypes associated with mtDNA deletions. To examine mitochondrial fusion, we expressed matrix-targeted photoactivatable GFP in control and patient fibroblasts (Karbowski *et al.*, 2004). After photoactivation of mitoPAGFP in a portion of mitochondria, we monitored mixing of the fluorescent matrix marker. We found that the fluorescence intensity of mitoPAGFP similarly decreased for 60 min in both fibroblasts, suggesting that mitochondrial fusion is not inhibited in patient fibroblasts (Fig.4).

Identification of a missense mutation in the *CHCHD10* gene by exome sequencing

Analysis of genes involved in multiple mtDNA deletions with a compatible phenotype (*POLG*, *SLC25A4*, *PEO1*) revealed no mutation. To identify the causative gene, we sequenced the exome of patients IV-11 and V-10. The procedure yielded 9.8 and 12.4 Gb of

For Peer Review

mappable sequence and after alignment to the hg19 reference genome, the average depth was ~70x and ~91x, respectively. From the 62 252 and 63 036 identified SNPs in patients IV-11 and V-10 respectively, the pathogenic variant was identified by the following scheme: (1) Selection of heterozygous variants shared by the 2 patients, (2) Exclusion of polymorphic variants present in dbSNP132, EVS (Exome Variant Server), HapMap, 1000 Genome databases and in-house control exomes (3) Segregation analysis within the family. This filtering led us to identify a single heterozygous missense mutation (c.176C>T; p.Ser59Leu) in exon 2 of *CHCHD10* that was present in the 8 patients tested and was absent in 2 healthy individuals (IV-14 and IV-16) with normal neurological examination at 79 and 69 years, respectively (Fig.5A-B). This gene encodes the coiled-coil helix coiled-coil helix domain-containing protein 10 whose function is unknown. However, the C-terminal CHCH domain is primarily seen in mitochondrial proteins and was known to be involved in the protein import and metal binding in the intermembrane space (Banci *et al.,* 2009). The mutation changes a highly conserved serine into a leucine and was not present in 200 ethnically and geographically matched control alleles (Fig.5C). *In silico* study by PolyPhen-2 (http://genetics.bwh.harvard.edu/pph2/), SIFT (http://sift.jcvi.org/) and Mutation Taster (http://www.mutationtaster.org/) predicted this variant to be probably damaging.

The CHCH domain of CHCHD10 is characterized by a CX_9C motif. Although all CX_9C proteins presumably preserve a disulfide bonded α-hairpin conformation, they have a large range of sequence lengths and a very low degree of sequence similarity both within or specific organism and the orthologs of different species (Longen *et al.,* 2009; Cavallo *et al.,* 2010). Therefore, these features do not allow to easily predict accurate structural models for this protein family. Recently, Banci *et al*. have structurally characterized two members of them, CHCHD5 and CHCHD7, in their fully oxidized states (Banci *et al.,* 2012). Using the same program, 142 residues of CHCHD10 (Met1 to Pro142) were modeled using CHCHD5

For Peer Review

as template (PDB ID: 2LQL). Swiss-Pdb Viewer 3.7 (http://www.expasy.org/spdbv) was used to analyze the structural insight into CHCHD10 mutation and visualize the structure. The modeling of CHCHD10 shows (i) a non-structured N-terminal region, (ii) a highly hydrophobic helix (Gly43 to Ala 68) which may be typically an interface of interaction with an interacting protein, (iii) and the CHCH domain near the C-terminal region characterized by a CX_9C motif (Fig.5D). The four cysteine residues (102, 112, 122 and 132) of the CHCH domain are involved in two disulfide bonds. The p.Ser59 is located in the hydrophobic N-terminal α-helix, and as the few other polar residues of this helix, it may intervene in hydrogen bonds to stabilize CHCHD10 interaction with another protein. Thus, the p.Ser59Leu mutation could possibly alter protein-protein interactions.

To investigate whether the p.Ser59Leu mutation has an effect on the expression of CHCHD10, we analysed CHCHD10 level in muscle of patients by western blotting. We used GAPDH and the mitochondrial SMAC protein as controls for quantitation. Normalization showed no significant reduction of CHCHD10 expression in patient muscles compared to control (not shown).

CHCHD10 is a mitochondrial protein located in the intermembrane space

First, we looked at the expression of CHCHD10 in human tissues by western blot. The protein is ubiquitous and highly expressed in organs with a high mitochondria content like the heart or liver (Fig.6A). Confocal microscopic analysis then showed a colocalization, in HeLa cells, of endogenous CHCHD10 with MitoTracker, a dye that accumulates specifically in mitochondria (Fig.6B). To analyze submitochondrial localization of CHCHD10, mitochondria isolated from HeLa cells were treated with proteinase K. Proteins inside mitochondria are protected from protease digestion. As shown in Figure 6C, CHCHD10 was resistant to treatment with proteinase K indicating that the protein is present inside mitochondria. As expected, the TOM20 protein (outer mitochondrial membrane) was digested by proteinase K

For Peer Review

while SMAC (intermembrane space) was resistant to protease digestion. Analysis of the mitochondrial preparations for PCNA and GAPDH confirmed the absence of nuclear and cytosolic contaminations, respectively. When mitochondria were subjected to alkali extraction, peripheral membrane proteins were recovered in the supernatant, while integral membrane proteins were found in the membrane-containing pellet fractions (Fig.6D). As expected, the outer membrane integral protein VDAC was primarily recovered in the pellet following extraction while SMAC was recovered in the supernatant. CHCHD10 was distributed in the supernatant indicating that it was located in the soluble fraction. Last, to discriminate between intermembrane space or matrix localization, mitochondria were treated with digitonin to open the inner membrane space. In the resulting mitoplasts, CHCHD10 was degraded by proteinase K like MFN2 (outer mitochondrial membrane), SMAC (intermembrane space) and mitofilin, an inner mitochondrial membrane protein mainly facing the intermembrane space, while Hsp60, which is located in the mitochondrial matrix, was protected against protease digestion (Fig.6E). All these results suggest that CHCHD10 is an intermembrane space protein.

CHCHD10 is enriched at cristae junctions

We performed immunogold labeling of chemically fixed cryosectioned HeLa cells (Fig.7A). The sections were labeled with a primary antibody against CHCHD10, followed by a secondary gold conjugate. For quantitative analysis, we determined the location of each gold particle (n = 229) with respect to the inner boundary membrane and the closest cristae membrane and plotted its respective localization in a model (Fig.7B). We found that the majority of mitochondrial gold particles were enriched in the vicinity of cristae junctions as reported previously for mitofilin, a major component of the MINOS complex (Jans *et al.,* 2013). We performed the same experiment with a primary antibody against Hsp60, a protein highly expressed in the matrix, as a control (Fig. 7C-D).

For Peer Review

Expression of CHCHD10 mutant leads to fragmentation of the mitochondrial network and to defect in cristae maintenance

To confirm the role of the p.Ser59Leu mutation, we analyzed the effects of overexpression of the pathogenic allele on mitochondrial network. HeLa cells were transiently transfected with the empty vector, the wild-type allele or the pathological allele. After transfection, HeLa cells produced equivalent amounts of wild-type and mutant CHCHD10 (Fig.8A). Mitochondrial network morphology and CHCHD10 labeling were next assessed using Mitotracker red and CHCHD10 antibodies, respectively. Forty eight hours after transfection with either empty vector or the wild-type allele, Mitotracker revealed a filamentous network. Overexpression of mutant CHCHD10^{S59L} altered mitochondrial morphology in transfected cells with a significant fragmentation of the network (Fig.8B-C). We also looked at the mitochondrial morphology by electron microscopy. Contrary to overexpression of either empty vector or the wild-type allele, overexpression of the CHCHD10^{S59L} mutant led to major abnormalities including loss, desorganization or dilation of cristae. Matrix condensation was also observed in numerous mitochondria (Fig.9A-D).

Involvement of the same *CHCHD10* mutation in an FTD-ALS family

The observation of a FTD-ALS phenotype in a mitochondrial disease led us to analyze *CHCHD10* variants in a cohort of 21 FTD-ALS families previously tested by exome sequencing. We identified the heterozygous c.176C>T (p.Ser59Leu) mutation in a patient whose family is originally from Catalonia (Spain). This man developed walking difficulties at 57 years of age. Progressively, he presented a pseudo-bulbar syndrome with dysarthria and dysphagia. Electromyography confirmed motor neuron involvement with symmetrical denervation predominent in muscles of the face but also in muscles of upper and lower limbs.

For Peer Review

Motor and sensory conduction velocities were normal. The patient also had cognitive impairment and behavioural changes suggesting a frontotemporal dementia. Neuropsychological testing revealed a frontal lobe dysfunction, notably impairment of conceptualization, perseverative behaviours and paraphasia with relative preservation of memory. Brain MRI showed mild bilateral frontal atrophy. Parkinsonian signs were also present with akinesia, rigidity and gait disorders and a UPDRS scale at 10. In addition, the patient presented bilateral sensorineural hypoacousia and a muscular fatigability. A total loss of autonomy was observed after 8 years of evolution, then he was loss sight. The elder sister and one brother of the index case presented ALS with predominant bulbar features and died after 4 years of evolution. Their father developed a neurological disease with progressive walking and speaking difficulties at 61 years of age leading to death 3 years later. No patient had a muscle biopsy. The presence of the mutation was confirmed by Sanger method in the index case but the absence of DNA samples from other family members did not allow to perform segregation analysis.

For Peer Review

DISCUSSION

In this study, we first identified a new gene involved in mtDNA instability disease. We describe a large family in which affected individuals carry a missense mutation in the *CHCHD10* gene. The clinical phenotype associated with this *CHCHD10* mutation is unusual because patients developed a late-onset disease, which begins around fifty, with highly variable clinical presentations. Affected individuals presented with either isolated or associated symptoms including ataxia, dementia and ALS-like presentation; the only element common to all patients being the presence of a mitochondrial myopathy with numerous ragged-red and COX-negative fibers associated with multiple mtDNA deletions. None of the affected individuals presented with an external ophtalmoplegia. A patient only (IV-15)

presented with a ptosis associated with facial palsy, probably due to motor neuron disease. In this family, the phenotype is really particular compared to those reported in mtDNA instability disorders. The course of the disease was highly variable, ranging from one to more than 15 years of evolution before death. However, it was more severe than the PEO (Progressive External Ophtalmoplegia) phenotypes classically observed in pedigrees with autosomal dominant transmission of multiple mtDNA deletions (Copeland, 2012). Cerebellar ataxia is exceptionnally observed in the absence of PEO in mtDNA instability disease, except in MIRAS or MSCAE phenotypes (Copeland, 2012), secondary to *POLG* mutations, or in IOSCA (Hakonen *et al.,* 2007), secondary to *TWINKLE* mutations. MND with ALS-like symptoms is even rarer with exceptional cases associated with *POLG*, *TK2* or *DGUOK* mutations (Ronchi *et al.,* 2012). The cognitive impairment observed in our family looks like frontotemporal dementia usually observed in ALS patients. This observation led us to analyse *CHCHD10* in FTD-ALS families with a dominant mode of transmission and to identify the same missense p.Ser59Leu mutation in one of these families. FTD-ALS is a genetically heterogeneous disorder and a hexanucleotide repeat expansion in a noncoding region of the chromosome 9 open reading frame 72 (*C9ORF72*) gene, the function of which is unknown, has been recently identified as a common cause of FTD-ALS (DeJesus-Hernandez *et al.*, 2001; Renton *et al.*, 2011). Patients with a *C9ORF72* expansion present with FTD, ALS, or both. Parkinsonism is common and the phenotype of our second family was highly evocative of a *C9ORF72* expansion. However, *C9ORF72* screening and the analysis of other candidate genes for ALS and FTD were negative in this family (*TARDBP, FUS/TLS, SOD1, VCP, CHMP2B, ANG, SQSTM1, UBQLN2, PFN1*). No patient had a muscle biopsy but it is likely that sensorineural hypoacousia and muscle weakness observed in the index case were related to mitochondrial dysfunction. Our study clearly shows that *CHCHD10* is a novel gene

For Peer Review

responsible for ALS-FTD clinical spectrum, which raises the intriguing prospect of an underlying mitochondrial basis for this group of disorders.

The function of CHCHD10 is unknown. However, it belongs to a family of mitochondrial proteins characterized by conserved CX_nX motifs (Banci *et al.,* 2009) and it is expected to be involved in oxidative phosphorylation (Martherus *et al.*, 2010). These proteins are incorporated into the intermembrane space and are then trapped through a redox-dependent protein machinery *via* the intermembrane space protein Mia 40 (CHCHD4) (Stojanovski *et al.,* 2012). CHCHD3 is a member of this family predominantly localized to the inner membrane, facing toward the intermembrane space (Darshi *et al.,* 2012). It is part of the large protein complex called as MINOS and plays a role in maintening mitochondrial function and cristae integrity (Darshi *et al.,* 2011; van der Laan *et al.,* 2012). OPA1 has been shown to be involved in regulating cristae remodeling independently of its role in mitochondrial fusion (Frezza *et al.,* 2006). CHCHD3 interacts both with OPA1 and mitofilin suggesting that it is a scaffolding protein that stabilizes complexes involved in maintening cristae architecture (Darshi *et al.,* 2011). Another member of this family, CHCM1/CHCHD6, is critical for maintening the cristae morphology, ATP production and oxygen consumption. It has the same localization than CHCHD3 and strongly interacts with mitofilin (An *et al.,* 2012). Here, we show that CHCHD10 is a mitochondrial protein, located in the intermembrane space. Unlike CHCHD3 and CHCM1/CHCHD6, which are inner membrane-associated proteins, CHCHD10 is a soluble protein. By electron microscopy, we also show that it is enriched at cristae junctions, like mitofilin, suggesting that it could be another actor in maintening cristae morphology. The cristae alterations found both in patient fibroblasts and HeLa cells overexpressing $CHCHD10^{S59L}$ mutant are also in favor of this hypothesis. There is a strong evidence that the mitochondrial F_1F_0-ATP synthase, apart from its enzymatic

For Peer Review

activity, plays a major role in determining the structure of cristae (Zick *et al.,* 2009). The regular arrangement of this highly abundant protein complex might serve as a kind of backbone stabilizing tubular cristae structures. On the contrary, we could ask whether the abnormal pattern observed for F_1F_0-ATP synthase by BN-PAGE analysis in the muscle of patients is not secondary to an abnormal organization of cristae linked to the p.Ser59Leu mutation. Furthermore, this mutation leads to a respiratory chain deficiency both in muscle and fibroblasts of patients suggesting that CHCHD10 is critical for maintening ATP production and oxygen consumption. It has been shown that cristae shape regulates respiratory chain supercomplexes stability and assembly with an impact on mitochondrial respiratory efficiency, thus suggesting that shape of biological membranes can influence membrane protein complexes (Cogliati *et al.,* 2013). Further experiments will be necessary to determine whether these effects of CHCHD10 mutant are linked to destabilization of cristae morphology.

Down-regulation of both *CHCHD3* and *CHCM1/CHCHD6* in HeLa cells resulted in fragmentation and clustering of the mitochondrial network (Darshi *et al.,* 2011; An *et al.,* 2012). This could indicate either increased fission or decreased fusion in knock-out cells. Studies with the dominant negative mutant of Drp1, $DRP1^{K38A}$, which blocks fission, suggested that the mitochondria in CHCHD3 knock-out cells have impaired fusion activity (Darshi *et al.,* 2011). Fibroblasts of patients carrying the *CHCHD10* mutated allele presented a fragmentation of the mitochondrial network and less connected mitochondria. However, a direct assay with a photoactivable mitochondrial form of GFP did not find a mitochondrial fusion defect in patient fibroblasts. The accumulation of mtDNA deletions in skeletal muscle can be secondary to an increase in mtDNA damage, a defect in mtDNA repair and/or a failure to clear mitochondria with damaged DNA (Chen and Chan, 2010). Recently, we have shown

For Peer Review

that fibroblasts bearing a *MFN2* mutation, responsible for optic atrophy 'plus' phenotype with mtDNA multiple deletions, have a lower capacity to repair stress-induced mtDNA lesions compared to control cells (Rouzier *et al.,* 2012). It is likely that the defect in mtDNA repair that we observed is due to defective fusion that leads to a variability in repair protein content across the mitochondrial population, thus contributing to mtDNA instability. Mitochondrial DNA instability found in patients carrying the p.Ser59Leu *CHCHD10* mutation cannot be explained by a fusion deficiency. However, mammalian cells contain thousands of copies of mtDNA assembled into hundreds of nucleoids that are closely associated with the inner membrane and often appear to be wrapped around cristae or crista-like inner membrane invaginations (Brown *et al.*, 2011). One cannot exclude that cristae alterations secondary to CHCHD10^{S59L} expression lead to nucleoid structure disorganization and contribute to defect of mtDNA maintenance.

In conclusion, our study has provided strong supporting evidence that the CHCHD10 protein plays a role in the maintenance of mitochondrial cristae morphology and mtDNA stability. Additonal work will be needed to clarify the pathogenic mechanisms linking *CHCHD10* mutations with these downstream deleterious consequences and ultimately, the observed neurodegenerative phenotype. Moreover, this work opens a novel field to explore the pathogenesis of FTD-ALS clinical spectrum by showing that mitochondrial disease may be at the origin of some of these phenotypes. The analysis of *CHCHD10* also needs to be performed in patients presenting with ALS or FTD in both sporadic and familial cases.

For Peer Review

ACKNOWLEDGEMENTS

We acknowledge Pasteur-IRCAN Cellular and Molecular Imaging platform (PICMI). We also acknowledge Pr François Tison (CHU Bordeaux), Cyril Goizet (CHU Bordeaux) and Pr Olivier Rascol (CHU Toulouse). This work was made possible by grants to V.P-F from the

Association Française contre les Myopathies (AFM) and the Fondation pour la Recherche Médicale (FRM), to H.S from National Institutes of Health (GM089853) and to A.B by the program "Investissements d'avenir" ANR-10-IAIHU-06, 'The Programme Hospitalier de Recherche Clinique' (to I.L.B.) and the 7th framework program of the European Union (FP7, E12009DD, Neuromics). P.YWM is supported by a Clinician Scientist Fellowship Award (G1002570) from the Medical Research Council (UK).

For Peer Review

REFERENCES

Amati-Bonneau P, Valentino M, Reynier P, Gallardo M, Bornstein B, Boissière A, et al. *OPA1* mutations induce mitochondrial DNA instability and optic atrophy 'plus' phenotype. Brain 2008; 131: 338-51.

An J, Shi J, He Q, Lui K, Liu Y, Huang Y, et al. CHM1/CHCHD6, a novel mitochondrial protein linked to regulation of mitofilin and mitochondrial cristae morphology. J Biol Chem 2012; 287: 7411-26.

Banci L, Bertini I, Ciofi-Baffoni S, Tokatlidis K. The coiled coil-helix coil-helix proteins may be redox proteins. FEBS Lett 2009; 583: 1699-702.

Banci L, Bertini I, Coffi-Baffoni S, Jaiswal D, Peruzzini R, Winkelman J. Structural characterization of CHCHD5 and CHCHD7: two atypical twin CX9C proteins. J Struct Biol 2012; 180: 190-200.

Bannwarth S, Figueroa A, Fragaki K, Destroismaisons L, Lacas-Gervais S, Lespinasse F, et al. The human *MSH5* (MutS Homolog 5) gene localizes to mitochondria and protects the mitochondrial genome from oxidative damage. Mitochondrion 2012; 12: 654-65.

Bradford M. A rapid and sensitive method for the quantitation of micrograms quantities of protein utilizing the principle of protein-dye binding. Annal Biochem 1976; 251: 69-72.

Brown TA, Tkachuk AN, Shtengel G, Kopek BG, Bogenhagen BF, Hess HF et al. Superresolution fluorescence imaging of mitochondrial nucleoids reveals their spatial range, limits and membrane interaction. Mol Cell Biol 2011; 31: 4494-5010.

Cavallo G. Genome-wide analysis of eukaryotic twin CX9C proteins. Mol Biosyst 2010; 6: 2459-70.

Chen H, Chan D. Physiological functions of mitochondrial fusion. Ann N Y Acad Sci 2010; 1201: 21-5.

Cogliati S, Frezza C, Soriano M, Varanita T, Quintana-Cabrera R, Corrado M, et al. Mitochondrial cristae shape determines respiratory chain supercomplexes and respiratory efficiency. Cell 2013; 155: 160-71.

Copeland W. Defects in mitochondrial DNA replication and human disease. Crit Rev Biochem Mol Biol 2012; 47: 64-74.

Darshi M, Mendiola V, Mackey M, Murphy A, Koller A, Perkins G, et al. ChChd3, an inner mitochondrial membrane protein, is essential for maintening crista integrity and mitochondrial function. J Biol Chem 2011; 286: 2918-32.

Darshi M, Trinh K, Murphy A, Taylor S. Targeting and import mechanism of coiled-coil helix coiled-coil helix domain-containing protein 3 (ChChd3) into the mitochondrial intermembrane space. J Biol Chem 2012; 287: 39480-91.

DeJesus-Hernandez M, Mackenzie IR, Boeve BF, Boxer AL, Baker M, Rutherford NJ et al. Expanded GGGGCC hexanucleotide repeat in noncoding region of C9ORF72 causeschromosome 9p-linked FTD and ALS. Neuron 2011; 72: 245-56.

Delettre C, Laeners G, Griffoin J, Gigarel N, Lorenzo C, Belenguer P, et al. Nuclear gene *OPA1*, encoding a mitochondrial dynamin-related protein, is mutated in dominant optic atrophy. Nat Genet 2000; 26: 207-10.

Frezza C, Cipolat S, Martins de Brito O, Micaroni M, Beznoussenko G, Rudka T, et al. OPA1 controls apoptotic cristae remodeling independently from mitochondrial fusion. Cell 2006; 126: 177-89.

Hakonen A, Isohanni P, Paetau A, Herva R, Suomalainen A, Lonngvist T. Recessive Twinkle mutations in early onset encephalopathy with mtDNA depletion. Brain 2007; 130: 3032-40.

Hudson G, Amati-Bonneau P, Blakely E, Stewart J, He L, Schaefer A, et al. Mutation of *OPA1* causes dominant optic atrophy with external ophtalmoplegia, ataxia, deafness, and multiple mitochondrial DNA deletions: a novel disorder of mtDNA maintenance. Brain 2008; 131: 329-37.

Jans D, Wurm C, Riedel D, Wenzel D, Stagge F, Deckers M, et al. STED super-resolution microscopy reveals an array of MINOS clusters along human mitochondria. PNAS 2013; 110: 8936-41.

Karbowski M, Arnoult D, Chen H, Chan DC, Smith CL, Youle RJ. Quantitation of mitochondrial dynamics by photolabeling of individual organelles shows that mitochondrial fusion is blocked during the Bax activation phase of apoptosis. J Cell Biol. 2004;164: 493-9.

Kelley L, Sternberg M. Protein structure prediction on the web: a case study using the Phyre server. Nat Protoc 2009; 4: 363-71.

Kim JS, Xu X, Li H, Solomon D, Lane WS, Jin T, Waldman T. Mechanistic analysis of a DNA damage-induced, PTEN-dependent size checkpoint in human cells. Mol Cell Biol. 2011;31: 2756-71.

For Peer Review

Koshiba T, Detmer S, Kaiser J, Chen H, McCaffery M, Chan D. Structural basis of mitochondrial tethering by mitofusin complexes. Science 2004; 305: 858-62.

Longen S, Bien M, Bihlmaier K, Kloeppel C, Kauff F, Hammermeister M, et al. Systematic analysis of the twin cx(9)c protein family. J Mol Biol 2009; 393: 356-68.

Martherus RSRM, Sluiter W, Timmer EDJ, VanHerle SJV, Smeets HJM, Ayoubi TAY. Functional annotation of heart enriched mitochondrial genes GBAS and CHCHD10 through guilt by association. Bioch Biophys Res Com 2010; 402: 203-208.

Meeusen S, McCaffery M, Nunnari J. Mitochondrial fusion intermediates revealed *in vitro*. Science 2004; 305: 1747-52.

Moraes C, DiMauro S, Zeviani M, Lombes A, Shanske S, Miranda A, et al. Mitochondrial DNA deletions in progressive external ophtalmoplegia and Kearns-Sayre syndrome. N Engl J Med 1989; 18: 1293-9.

Naimi M, Bannwarth S, Procaccio V, Pouget J, Desnuelle C, Pellissier J, et al. Molecular analysis of *ANT1, TWINKLE* and *POLG* in patients with multiple deletions or depletion of mitochondrial DNA by dHPLC-based assay. Eur J Hum Genet 2006; 14: 917-22.

Paul R, Santucci S, Saunières S, Desnuelle C, Paquis-Flucklinger V. Rapid mapping of mitochondrial DNA deletions by large-fragment PCR. Trends Genet 1996; 12: 131-2.

Renton AE, Majounie E, Waite A, Simon-Sanchez J, Rollinson S, Gibbs JR et al. A hexanucleotide repeat expansion in C9ORF72 is the cause of chromosome 9p21-linked ALS-FTD. Neuron 2011; 72: 257-68.

Ronchi D, Garone C, Bordoni A, Rios PG, Calvo SE, Ripolone M et al. Next-generation sequencing reveals *DGUOK* mutations in adult patients with mtDNA deletions. Brain 2012; 135 : 3404-3415.

Rouzier C, Bannwarth S, Chaussenot A, Chevrollier A, Verschueren A, Bonello-Palot N, et al. The *MFN2* gene is responsible for mitochondrial DNA instability and optic atrophy 'plus' phenotype. Brain 2012; 135: 23-34.

Rouzier C, Le Guédard-Méreuze S, Fragaki K, Serre V, Miro J, Tuffery-Giraud S, et al. The severity of phenotype linked to *SUCLG1* mutations could be correlated with residual amount of SUCLG1 protein. J Med Genet 2010; 47: 670-6.

Rustin P, Chretien D, Bourgeron T, Gerard B, Rotig A, Saudubray J. Biochemical and molecular investigations in respiratory chain deficiencies. Clin Chem Acta 1994; 228: 31-51.

Schägger H, Pfeiffer K. The ratio of oxidative phosphorylation complexes I-IV in bovine heart mitochondria and the composition of respiratory chain supercomplexes. J Biol Chem 2001; 276: 37861-7.

Shapira A. Mitochondrial diseases. Lancet 2012; 379: 1825-34.

For Peer Review

Smirnova E, Shurland D-L, Ryazantsev S, van der Blieck A. A human dynamin-related protein controls the distribution of mitochondria. J Cell Biol 2001; 143: 351-8.

Song Z, Ghochani M, McCaffery M, Frey T, Chan D. Mitofusins and OPA1 mediate sequential steps in mitochondrial membrane fusion. Mol Biol Cell 2009; 20: 3525-32.

Stojanovski D, Bragozewski P, Chacinska A. The Mia pathway: A tight bond between protein transport and oxidative folding in mitochondria. BBA 2012; 1823: 1142-50.

Suomalainen A, Isohanni P. Mitochondrial DNA depletion syndromes-many genes, common mechanisms. Neuromuscul Disord 2010; 20: 429-37.

van der Laan M, Bohnert M, Wiedemann N, Pfanner N. Role of MINOS in mitochondrial membrane architecture and biogenesis. Trends Cell Biol 2012; 22: 185-92.

Wakabayashi J, Zhang Z, Wakabayashi N, Tamura Y, Fukaya M, Kensler TW, Iijima M, Sesaki H. The dynamin-related GTPase Drp1 is required for embryonic and brain development in mice. J Cell Biol 2009;186: 805-16.

Ylikallio E, Suomalainen A. Mechanisms of mitochondrial disease. Ann Med 2012; 44: 41-59.

Zanna C, Ghelli A, Porcelli A, Karbowski M, Youle R, Schimpf S, et al. *OPA1* mutations associated with dominant optic atrophy impair oxidative phosphorylation and mitochondrial fusion. Brain 2008; 131: 352-67.

Zick M, Rabl R, Reichert A. Cristae formation-linking ultrastructure and function of mitochondria. BBA 2009; 1793: 5-19.

Zuchner S, Mersiyanova I, Muglia M, Bissar-Tadmouri N, Rochelle J, Dadali E, et al. Mutations in the mitochondrial GTPase mitofusin 2 cause Charcot-Marie-Tooth neuropathy type 2A. Nat Genet 2004; 36: 459-1.

For Peer Review

LEGENDS TO FIGURES

Figure 1. Pedigree of the first family. Solid symbols represent clinically affected individuals. * corresponds to individuals tested for segregation analysis.

Figure 2. Muscle analysis. A-B. Histopathology with Gomori modified trichrome (A) showing RRFs and COX/SDH stain (B) revealing COX-deficient fibres, which are recognized by the prevalent blue stain. **C.** Ultrastructure of skeletal muscle showing abnormal mitochondria with cristalloid inclusions (arrows) **D.** Blue native electrophoresis of muscle

homogenates. Equal amounts (15 µg) of mitochondrial protein from age-matched control subjects (C) and patients IV-3 and V-2 were subjected to BN-PAGE, blotted onto a PVDF membrane and then incubated with specific antibodies. * corresponds to supplementary bands detected by anti-complex V antibody. **E.** Southern blot analysis revealing multiple deletion bands in addition to wild-type fragments in muscle of patients III-2, IV-11, IV-6 and V-2. C, control individual.

Figure 3. Mitochondrial fragmentation and ultrastructural alterations in skin fibroblasts. A. Cells obtained from a control (left panel) and patient V-10 (right panel) were analyzed by confocal microscopy using MitoTracker Red. Enlarged details of the areas are indicated. **B.** Mitochondrial phenotypes showed in A were quantified for 35 randomly-selected individual cells per each studied fibroblast cell line from 2 independent experiments. The data obtained were used to calculate the total length of the mitochondrial network per cell (left panel) and the average mitochondrial fragment length (right panel). Differences between the 2 cell lines were analyzed by Student's *t* test: significant (*: $0.05>p>0.01$), very significant (**: $0.01>p>0.001$) or extremely significant (***: $p<0.001$). **C-E.** Ultrastructural analysis of control (C) and patient V-10 (D-E) fibroblasts. Scale bar : 1µm **C.** Representative image of mitochondria with typical normal aspect found in control cells. **D.** Complete mitochondrial disorganization only found in patient cells. **E.** Moderate disorganization mainly found in patient cells.

Figure 4. Fusion analysis in patient fibroblasts. Control and patient fibroblasts expressing mitochondria-targeted photoactivatable GFP (mitoPAGFP) were stained with 7 nM tetramethylrhodamine ethyl ester (TMRE). mitoPAGFP was photoactivated with 405-nm laser in a small region of cells (30 x 30 pixels) at 0 min. Fibroblasts were observed with 15-min intervals for 60 min. Fluorescence intensity of mitoPAGFP was quantified using NIH Image J. Values represent the mean ± SME (n = 7 for control and 9 for patient).

For Peer Review

Figure 5. Identification of the p.Ser59Leu mutation in *CHCHD10*. A. Schematic representation of the exome data analysis and data filtering. NS: non-synonymous variants; SS: splice site disrupting single nucleotide variants; I: exonic indels. Known variants correspond to SNPs and Indels already reported in dbSNP132, EVS (Exome Variant Server), HapMap, 1000 Genome databases and in-house control exomes. **B.** *CHCHD10* mutation sequences in patients III-2, IV-3, IV-6, IV-11, IV-13, IV-15, V-2, V-10 and a control (WT). **C.** Cross-species protein conservation of CHCHD10, flanking the altered amino acid p.Ser59. **D.** Model of CHCHD10 based on the CHCHD5 structure (PDB ID: 2LQL). Aliphatic, polar, basic and acidic residues are respectively in grey, black, blue and red. Disulfide bonds are in green. The polar residue Serine 59 is indicated with an asterisk.

Figure 6. Mitochondrial localization of CHCHD10. A. Expression of CHCHD10 protein in human tissues analyzed by western blotting using human multiple tissue blot. **B.** Colocalization of endogenous CHCHD10 protein with MitoTracker Red indicating mitochondrial localization for CHCHD10 in HeLa cells (overlay in yellow). **C.** Intact isolated mitochondria from HeLa cells (lanes 1-4) were incubated in presence (+) or in absence (-) of Proteinase K or Triton X-100 before analysis by immunoblotting using antibodies against CHCHD10, TOM20 (mitochondrial outer membrane protein) or SMAC (mitochondrial intermembrane space protein). To verify the purity of isolated mitochondria, total lysates (lane 5) and mitochondrial isolates (lane 6) were analyzed by immunoblotting using antibodies against CHCHD10, GAPDH (cytosolic protein) or PCNA (nuclear protein). **D.** Intact mitochondria were prepared and subjected to Na_2CO_3 extraction. A soluble protein fraction (S) and an integral membrane protein fraction (P) were prepared. Samples of an extract from intact mitochondria (input), and the fraction of each extraction were subjected to western blot analysis. VDAC and SMAC were used to identify behaviors of well defined mitochondrial proteins that are integral membrane protein and soluble, respectively. **E.**

For Peer Review

Isolated mitochondria from HeLa cells (lanes 1-2) were incubated in presence (+) or in absence (-) of Digitonin or Proteinase K before analysis by immunoblotting using antibodies against CHCHD10, MFN2 (outer membrane protein), mitofilin (inner membrane protein mainly facing the intermembrane space), SMAC (intermembrane space protein) or Hsp60 (mitochondrial matrix protein).

Figure 7. Submitochondrial localization of CHCHD10 using immunoelectron microscopy. A. Immunogold labeling of CHCHD10 in HeLa cells. Arrows point to the position of gold particles. Enlarged details of the areas are indicated by black boxes. Scale bar: 500nm. **B.** Localization of the gold particles as determined by immunogold labeling of CHCHD10 plotted on a scheme representing a part of a mitochondrion. OM, outer membrane; IM, inner membrane. The histogram shows the fraction of gold particules within the indicated distance to the cristae junction. The histogram and the graphical representation are based on the same measured gold particle localizations. **C**. Control immunogold labeling of Hsp60 in HeLa cells. Scale bar: 500nm. **D.** Localization of the gold particles as determined by immunogold labeling of Hsp60 plotted on a scheme representing a part of a mitochondrion. OM, outer membrane; IM, inner membrane. The histogram shows the fraction of gold particules within the indicated distance to the cristae junction. The histogram and the graphical representation are based on the same measured gold particle localizations.

Figure 8. Effects of overexpression of wild-type and pathogenic CHCHD10 alleles on mitochondrial network in HeLa cells. Transfections were performed with empty vector (EV) or vectors encoding either wild-type CHCHD10-Flag (WT) or mutant CHCHD10-Flag (S59L). **A.** Western blot on HeLa cells extracts using antibodies against Flag, CHCHD10 or β-tubulin. NS, non specific. **B.** Analysis of DAPI (blue), Mitotracker (red) staining and CHCHD10 (green) immuno-labeling by fluorescence microscopy in HeLa cells transfected with either wild-type CHCHD10-Flag (WT) or mutant CHCHD10-Flag (S59L). **C.**

For Peer Review

Quantification of mitochondrial phenotypes of cells transfected with empty vector (EV) or vectors encoding either wild-type CHCHD10-Flag (WT) or mutant CHCHD10-Flag (S59L). Thirty five randomly-selected individual cells per each transfection were analyzed from 2 independent experiments. The data obtained were used to calculate the total length of the mitochondrial network per cell. Differences between the 2 cell lines were analyzed by Student's *t* test: very significant (**: $0.01>p>0.001$) or extremely significant (***: $p<0.001$).

Figure 9. Effects of overexpression of wild-type and pathogenic CHCHD10 alleles on cristae morphology in HeLa cells. **A.** Representative image of mitochondria after transfection with the empty vector. **B**. Representative image of mitochondria in cells overexpressing the wild-type CHCHD10 allele. **C-D.** Representative images of mitochondria in cells overexpressing the mutant CHCHD10 allele (S59L).

Table 1. Clinical data of affected members. M, male ; F, female ; AO, Age at onset ; AB, age at biopsy ; AD, age of death ; †, deceased; ?, unknown ; m, muscle; MND, motor neuron disease ; RRF, ragged-red fibers; COX-, COX negative fibers ; ↓, decreased; +, present; -, absent.

Table 2. Respiratory chain analysis in patient fibroblasts A-B. Spectrophotometric analysis of the respiratory chain enzyme activities in patient fibroblasts in glucose (A) and in galactose medium (B). CS, citrate synthase. Results are expressed as extreme absolute values or absolute values for controls or patients, respectively. Values are expressed in nanomols of substrate per minute per milligram of proteins (lowered values are in grey). **C-D.** Polarographic analysis of the respiratory chain in patient fibroblasts in glucose (C) and in galactose medium (D). G3P, glycerol 3-phosphate. Results are expressed as extreme absolute values or absolute values for controls or patients, respectively. Values are expressed in nanomols of oxygen per minute per milligram of proteins (lowered values are in grey).

For Peer Review

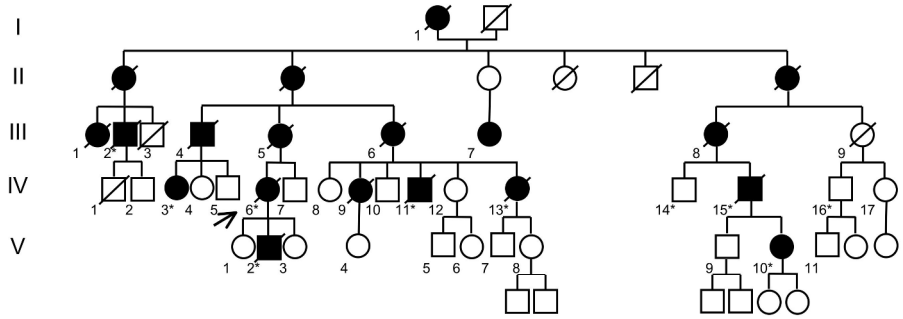

Figure 1

For Review

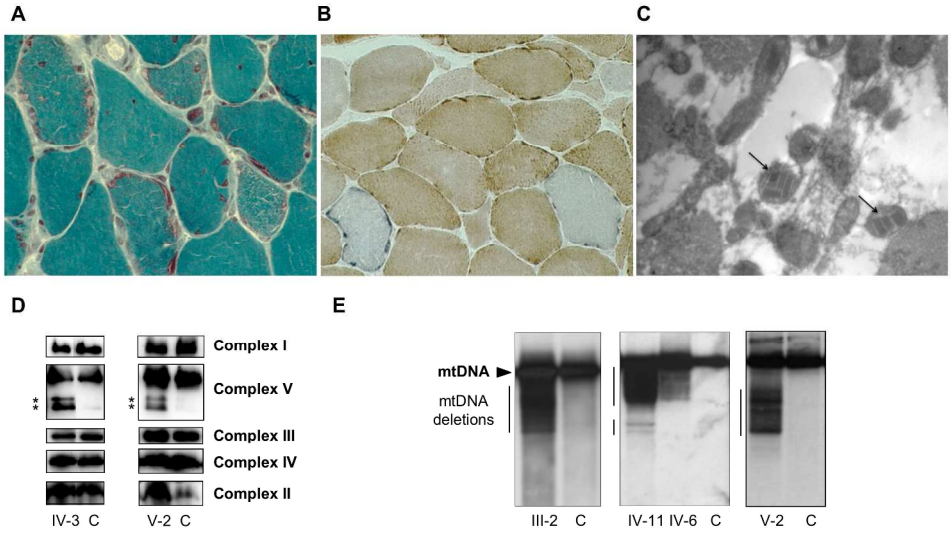

Figure 2

er Review

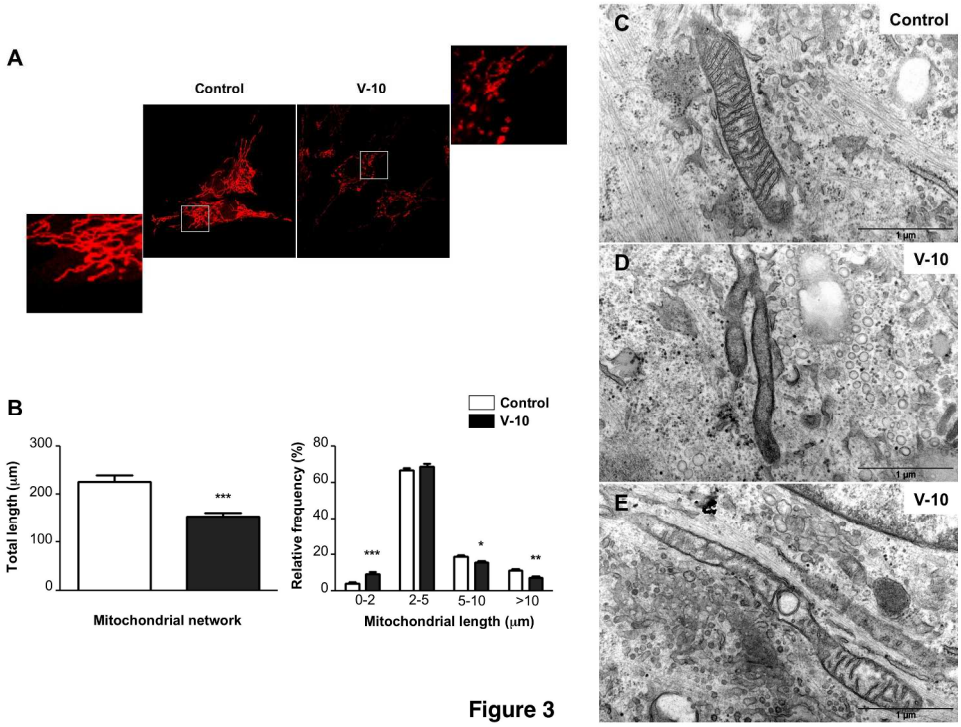

Figure 3

For Review

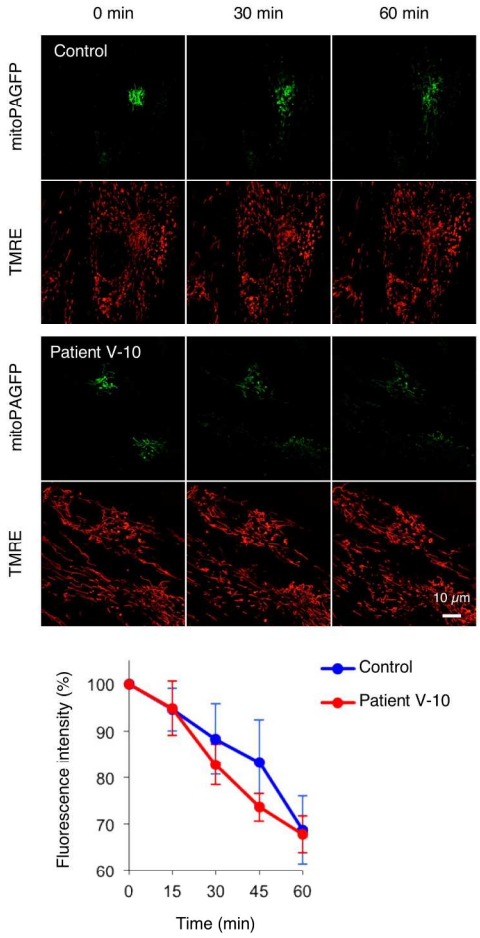
0 min
30 min
60 min
Control
mitoPAGFP
TMRE
Patient V-10
mitoPAGFP
TMRE
10 μm
Control
Patient V-10
Fluorescence intensity (%)
100
90
80
70
60
0
15
30
45
60
Time (min)

Figure 4

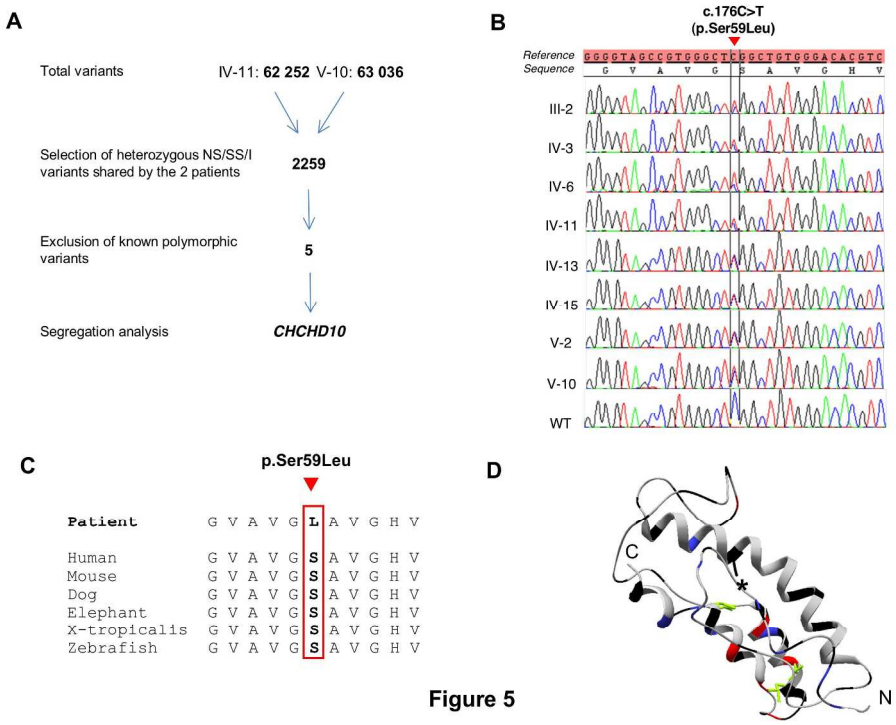

Figure 5

For Review

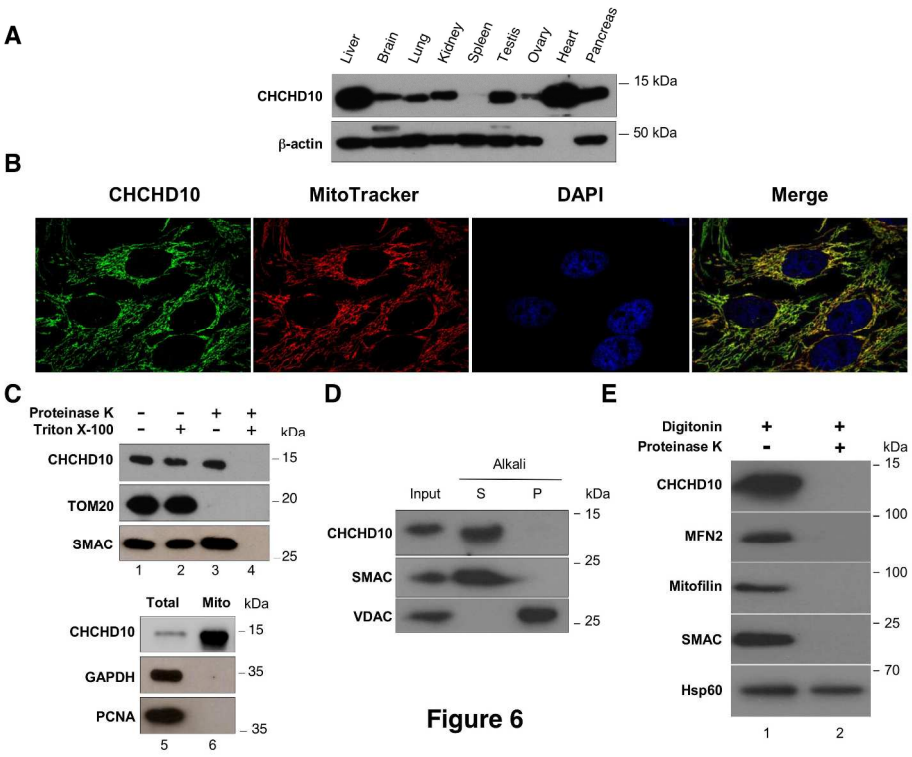

Figure 6

For Review

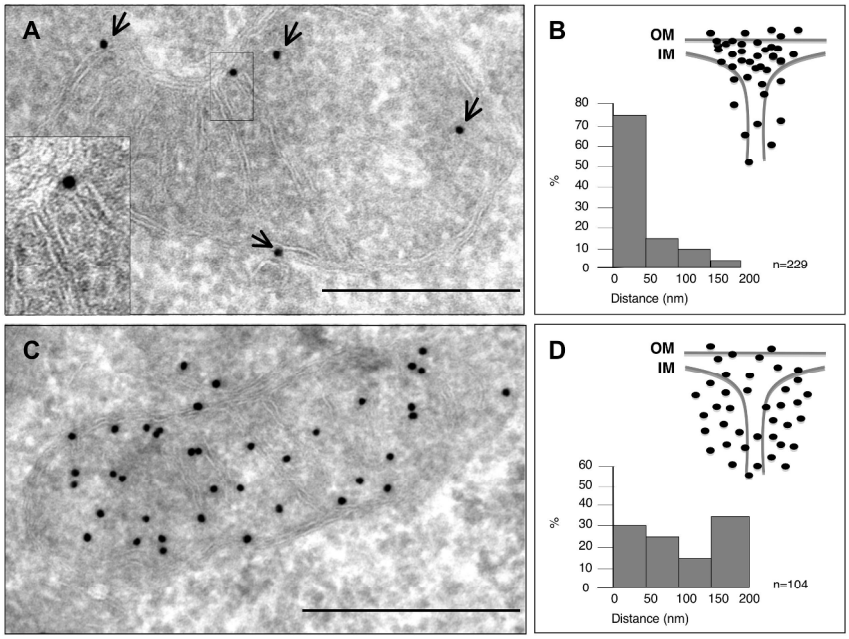

Figure 7

For Review

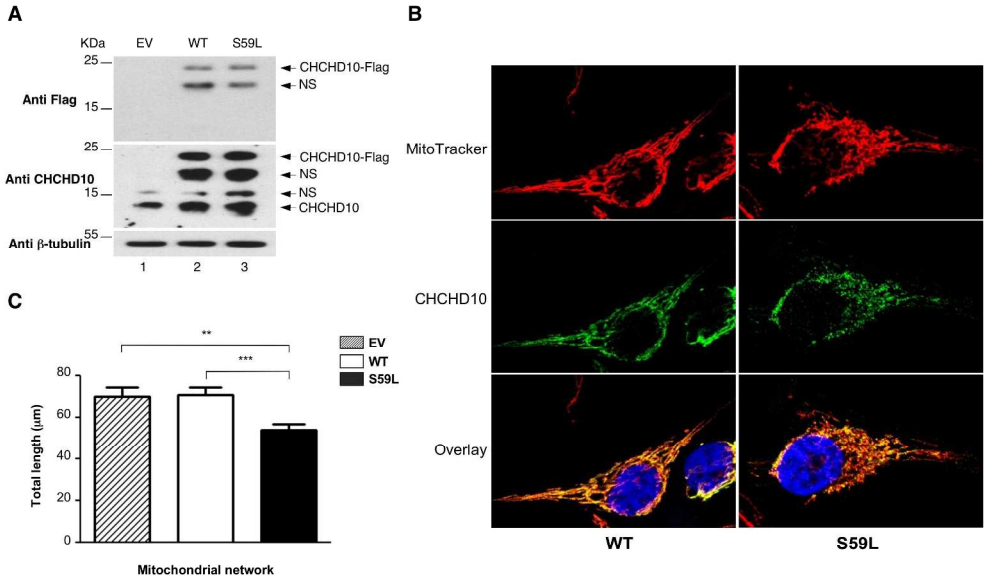

Figure 8

er Review

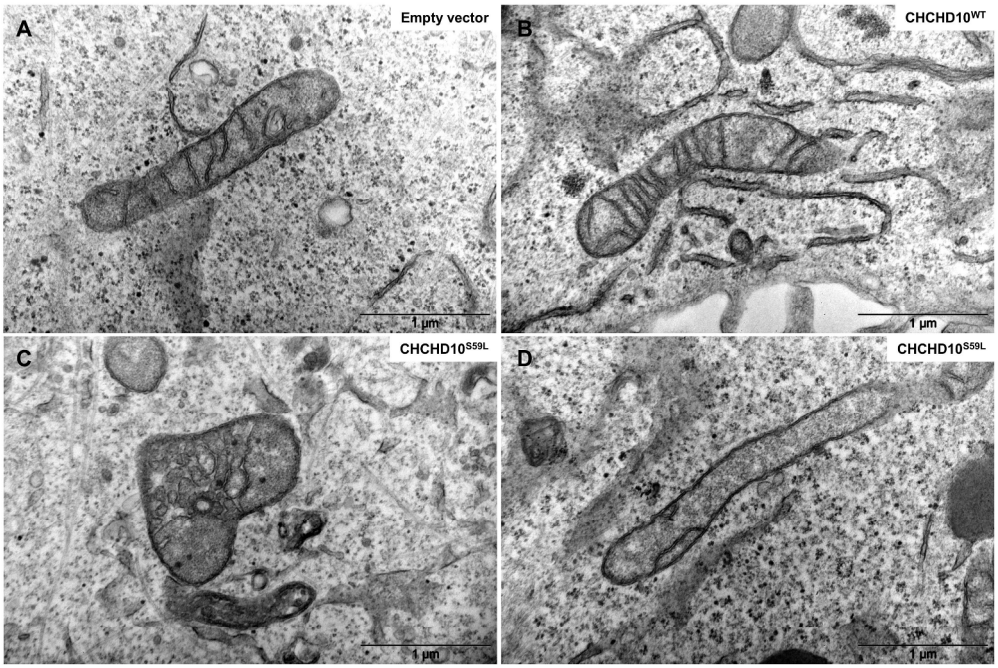

Figure 9

For Review

	III-2	IV-3	IV-6	IV-11	IV-13	IV-15	V-2	V-10
Sexe	M	F	F	M	F	M	M	F
AO (years)	?	65	50	58	60	50	50	49
AB (years)	78	68	67	63	62	75	50	50
AD (years)	† ?	-	67	70	† ?	77	51	-
Syndromic diagnosis	MND	MND + cerebellar syndrome	MND + cerebellar syndrome	MND	Cerebellar syndrome	MND + cerebellar syndrome	MND with ALS-like	Cerebellar syndrome
Cerebellar ataxia	-	+	+	-	+	+	-	+
Dysarthria	Bulbar	Bulbar	Bulbar+cerebellar	Bulbar	Cerebellar	Bulbar	Bulbar	Cerebellar
Dysphagia	Bulbar	Bulbar	Bulbar	Bulbar	-	Bulbar	Bulbar	-
Areflexia	+	+	+	?	?	+	+	+
Babinski sign	+	+	+	-	+	+	-	+
Cognitive impairment	+	+	+	+	+	+	-	+
Others	Deafness	Proximal weakness	Deafness	Proximal weakness	Proximal weakness, neurogenic bladder	Proximal weakness, ptosis, facial paresis	-	-
Muscle histology	RRF++ COX-	RRF++ COX-	RRF 30% COX- lipid and glycogen accumulation	RRF 30% COX- 40% lipid and glycogen accumulation	RRF 30% COX- lipid accumulation	RRF ++ COX- lipid accumulation	RRF 20% COX- 20% lipid accumulation	RRF++ COX- 15% lipid and glycogen accumulation
Respiratory chain analysis	↓CI, ↓CIV(m)	↓CIII (m)	↓CI, ↓CIV (m)	↓CI, ↓CIV (m)	Not done	Normal (m)	↓CI, ↓CIII, ↓CIV, ↓CV (m)	Normal (m)
mtDNA deletions	+ (m)	+ (m)	+ (m)	+ (m)	+ (m)	+ (m)	+ (m)	+ (m)

Table 1

For Peer Review

A

SPECTROPHOTOMETRIC ANALYSIS ON FIBROBLASTS						
GLUCOSE MEDIUM						
Enzymatic activities	**I**	**II**	**III**	**IV**	**V**	**CS**
Control values (nmol/min/mg of proteins)	9.0-27.1	18.5-54.0	57.4-176.2	109.9-350.0	22.0-46.2	74.7-161.1
Patient V-10	16.8	29.7	112.3	202.7	29.7	125.6

B

SPECTROPHOTOMETRIC ANALYSIS ON FIBROBLASTS						
GALACTOSE MEDIUM						
Enzymatic activities	**I**	**II**	**III**	**IV**	**V**	**CS**
Control values (nmol/min/mg of proteins)	15.2-19.4	28.2-33.1	88.8-116.4	181.7-315.4	22.7-32.1	124.8-223.0
Patient V-10	**10.0**	**26.7**	**60.2**	**167.1**	28.2	177.0

C

OXYGRAPHIC ANALYSIS ON FIBROBLASTS				
GLUCOSE MEDIUM				
	Oxygen consumption			
	Intact cells	**Digitonin permeabilized cells**		
		Glutamate+Malate	**Succinate**	**G3P**
Control values (nmol O2/min/mg of proteins)	5.90 - 13.80	8.00 - 16.60	8.00 - 15.80	4.90 - 13.50
Patient V-10	9.40	15.36	9.40	7.04

D

OXYGRAPHIC ANALYSIS ON FIBROBLASTS				
GALACTOSE MEDIUM				
	Oxygen consumption			
	Intact cells	**Digitonin permeabilized cells**		
		Glutamate+Malate	**Succinate**	**G3P**
Control values (nmol O2/min/mg of proteins)	5.58 – 8.25	8.16 – 9.91	8.60 – 9.76	5.22 – 12.91
Patient V-10	**4.66**	**6.22**	**7.82**	8.31

Table 2

For Peer Review

BRAIN-2014-00021

Responses to referees

All the experiments requested by the referees have been performed and their comments improved the impact of the manuscript in terms of clinical and pathogenesis. Identifying the *CHCHD10* involvement in FTD-ALS led us to change the title of the paper.

Referee 1

1) « *The BN-PAGE in Fig. 2D shows an instability of complex V, with the appearance of a smaller complex in the patients. The authors describe this finding as abnormal assembly of Complex V. Can they distinguish between a defect in assembly or increased instability? Which detergent and at which concentration has been used for these experiments? The levels of assembled complex II in the control (right panel) are much lower than in the patient. What is the evidence that the samples are equally loaded? The activity of complex V was normal in the patient fibroblast, even in galactose. The authors should comment on that. What about BN-PAGE in fibroblasts? Does it show the same result?* »

- We agree that smaller complexes observed with antibody against complex V can be secondary either to an abnormal assembling or to a degradation and it is not possible to distinguish between these two possibilities. This alternative has been added in the text.
  Page 13 - Lines 15,16: BN-PAGE assay of patients IV-3 and V-2 revealed smaller bands with antibody against complex V corresponding to assembly defect or increased instability (Fig.2D).
  Page 21 – Lines 23-25, Page 22- Line1 : On the contrary, we could ask whether the abnormal pattern observed for F_1F_0-ATP synthase by BN-PAGE analysis in the muscle of patients is not secondary to an abnormal organization of cristae linked to the p.Ser59Leu mutation.

- Solubilisation was performed in a solution of 1.5 M aminocaproic acid, 75 mM BIS-TRIS and 4% dodecyl-β-D-maltoside. These informations have been added in the patients and methods paragraph (**Page 6, Lines 12-14**)

- All revelations observed on figure 2D have been performed on the same gel after a sequential use of the 5 different antibodies. The evidence that the samples are equally loaded is showed by CI, CIII and CIV signals. Regarding CII, it is likely that the signal is not low in the patient V-2 but higher than in the control. The results of spectrophotometry in the muscle of this patient are in favour of this hypothesis with a high activity of CII (63.1 nmol/min/mg of proteins with control values between 20 and 65). This could reflect a compensatory mechanism corresponding to a mitochondrial proliferation, as it is frequently observed for example in patients presenting a mtDNA depletion leading to a multiple RC deficiency, except for nuclear encoded CII. We have not enough arguments to comment on this point but the sentence in the patients and methods paragraph has been completed. Page 6, Lanes 15-19 : Then they were electroblotted onto a PVDF membrane, prior to sequential incubation with specific antibodies directed against GRIM19 subunit of complex I, SDHA subunit of complex II, UQCRC2 subunit of complex III, MTCO1 subunit of complex IV and ATP5A subunit of complex V (Mitosciences) allowing to verify that samples were equally loaded between patients and controls.

- Mitochondrial disorders are characterized by tissue specificity. In most patients, a decreased activity of RC in muscle is not found in fibroblasts. Furthermore, in

For Peer Review

patients IV-3 and V-2, we observed smaller complexes with antibody against ATP5A but the band corresponding to normal size is not weaker in patients than in controls. So, this result does not necessarily imply a decrease in activity of complex V.

- We performed BN-PAGE analysis in patient fibroblasts. The assay did not reveal any abnormality including CV, the activity of which was normal by spectrophotometry. We mentioned this result in the text without showing the blot, which is presented below for the referee.
  Page 13, Lines 15-16 : BN-PAGE analysis of patient fibroblasts revealed no abnormality including complex V (not shown), the activity of which was normal by spectrophotometry.

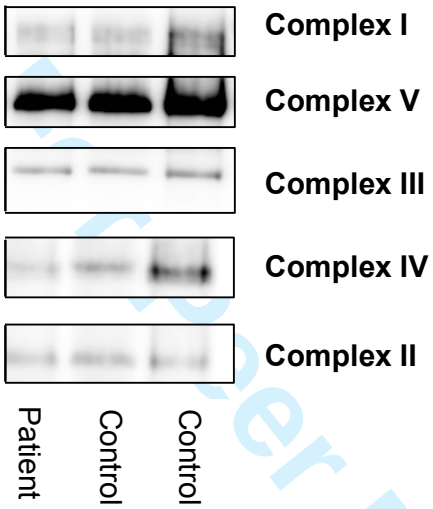

2) « *The western blot in Figure 5 is not of sufficient quality to be convincing. The loading of the samples shows discrepancy when using GAPDH or SMAC. Moreover, the OPA1 blotting does not show the expected long and short isoforms (important as the authors claim a defect in fusion). This western blot should be repeated to obtain convincing results, or it is better to omit it.* »

- It was not possible to make another blot because we have no more muscle samples available from patients. As it is requested by the referee, we deleted the figure 5. However, the information regarding the absence of a significant reduction of CHCHD10 expression (after normalization on 3 independent experiments) is still mentioned (as data not shown) because of its importance.

3) « *The enrichment of CHCHD10 at cristae is very interesting. However, the authors should also show a control image and quantification using an unrelated antibody. Moreover, in the quantification, what how is the distance from cristae defined? Is cristae morphology affected in cells overexpressing the mutant or downregulated for CHCHD10*? »

- In figure 7, a control image has been added showing immunogold labeling of Hsp60, a protein located in the mitochondrial matrix.
  Page 17, Lines 22-23 : We performed the same experiment with a primary

For Peer Review

antibody against Hsp60, a protein highly expressed in the matrix, as a control (Fig. 7C-D).

- For quantitative analysis, we determined the localization of each mitochondrial gold particle with respect to the inner boundary membrane and the closest cristae membrane and plotted its respective localization in a model. This information has been added in the text (**Page 17, Lines 17-19**).

- The empty vector, the wild-type allele or the pathological allele were tranfected in HeLa cells and we analyzed cristae morphology by electron microscopy. Overexpression of mutant CHCHD10^{S59L} altered mitochondrial morphology with loss, desorganization or dilation of cristae. A novel figure (Fig.9A-D) has been added to show these results.
  Page 18, Lines 9-13 : We also looked at the mitochondrial morphology by electron microscopy. Contrary to overexpression of either empty vector or the wild-type allele, overexpression of the CHCHD10^{S59L} mutant led to major abnormalities including loss, desorganization or dilation of cristae. Matrix condensation was also observed in numerous mitochondria (Fig.9A-D).

- Last, we also found mitochondrial ultrastructural alterations in patient fibroblasts. Data have been added in figure 3C-E.
  Page 14, Lines 1-9 : We then performed ultrastructural analysis of patient fibroblasts. Typical mitochondria of control cells had numerous, thin, well‑defined cristae, running perpendicularly to the mitochondrial longitudinal axis, and with a regular pattern of parallel organization (Fig.3C). They represented 90% of the mitochondrial profiles seen in two independent, genotype-blind, analyses of control cells. In patient cells, they represented 35% of the mitochondrial profiles. Completely disorganized mitochondria with sparse or absent cristae without recognizable parallel orientation were only observed in patient fibroblasts (18%) (Fig.3D). Less disorganized mitochondria represented 47% of the mitochondrial pattern in patient cells and 10% in control cells (Fig.3E).

4) « *In Figure 8A, the authors should comment on the band below the specific one that appears after transfection and is recognized both by the FLAG and the specific antibody* ».

- We agree that we did not enough explored the significance of this smaller band recognized both by the Flag and the specific antibody that are directed against the C-terminal part of the overexpressed and the endogenous proteins. It was not possible to exclude that this band could correspond to a specific isoform generated *via* downstream alternative translation initiation (dATI) (Kazak et al. 2012) occuring from AUG encoding methionines 45 or 48 of CHCHD10. To test this hypothesis, we mutated Flag-tagged CHCHD10 at codon 45 or 48 and overexpressed the corresponding plasmids in HeLa cells. The western blot below shows that the smaller band is also observed in the absence of internal methionine 45 or 48. This result suggests that it likely corresponds to a non specific signal with a possible N-terminal degradation.

For Peer Review

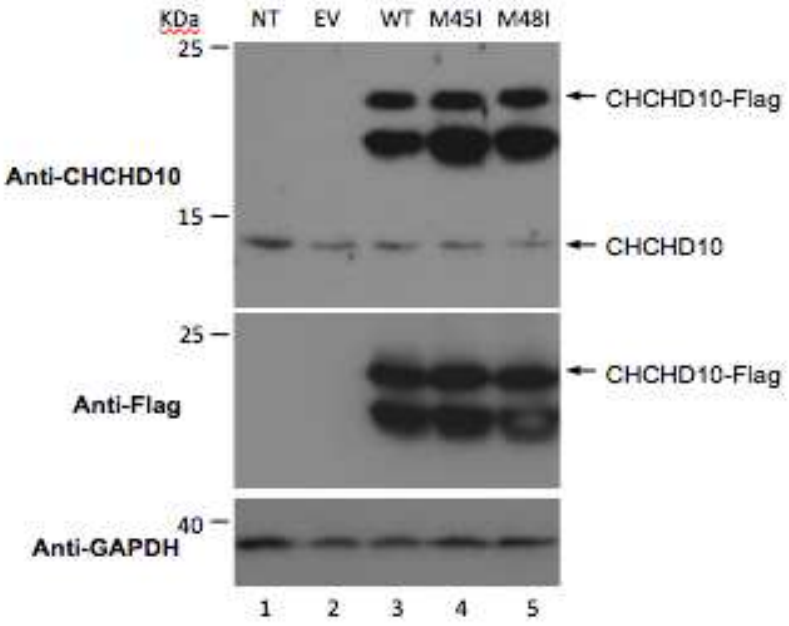

Western blot on HeLa cells extracts using antibodies against Flag, CHCHD10 or GAPDH. Transfections were performed with empty vector (EV) or vectors encoding either wild-type CHCHD10-Flag (WT), mutant CHCHD10-Flag (M45I) or mutant CHCHD10-Flag (M48I). NT : non transfected.

We added NS (Non Specific Signal) on the blot now presented in figure 8A.

5) « *The experiment shown in Figure 9 is not convincing in the present form. The authors should use a tagged version of DRP1-K38A to perform these experiments and use anti-tag antibody to detect transfected cells. The panel should also show control untransfected cells and cells transfected with the dominant-negative DRP1 alone (here dramatic elongation of the network should be visible). In the current experiment, it is remarkable that even in the presence of WT CHCHD10 the mutant DRP1 does not produce elongation of the mitochondrial network. This could mean that also transfection of WT protein affects fusion, or that the authors are not imaging the right cells. In the text the mutant Drp1 is described as resistant to fission. This is misleading. In reality this is a dominant-negative version of the protein that blocks fission, thus allowing the evaluation of unbalanced fusion. This assay is very indirect. A more direct way to look at mitochondrial fusion would be transfection of a photoactivable form of GFP followed by monitoring diffusion of the fluorescence in live imaging after photoactivation of a small portion of the network. This is an important point, since the authors conclude that CHCHD10 is involved in fusion* ».

- We agree that DRP experiment, that was used to support the hypothesis that *CHCHD10* was involved in mitochondrial fusion, is an indirect and inaccurate experiment. We performed the direct assay requested by the referee and we did not find a mitochondrial fusion defect in patient fibroblasts. The DRP experiment has been deleted and has been replaced by these data shown now in figure 4 with a corresponding paragraph in result section (**Page14, Lines 10-19).**

6) « *One final comment: localization of CHCHD10 in mitochondria, and a role in complex IV activity were previously described by Martherus et al., BBRC, 2010. It would be fair to cite this paper in the discussion*».

- This has been done.
  Page 20 - Lines 24-25, Page 21 - Line 1 : However, it belongs to a family of mitochondrial proteins characterized by conserved CX_nX motifs (Banci *et al.,* 2009) and it is expected to be involved in oxidative phosphorylation (Martherus *et al.*, 2010).

Referee 2

1) « *The clinical description of the patients indicates that areflexia and pyramidal signs are present together in several patients. What kind of pyramidal signs do the authors mean? Pyramidal involvement would rather lead to increased reflexes, this is why I would like to clarify this point* ».

- We agree that this point needs to be clarified and in fact pyramidal signs that we observed corresponded to Babinski sign, which suggested a motoneurone disease when associated with areflexia. « Pyramidal signs » has been replaced by « Babinski sign » both in the text and table 1.

2) « *It would be good to clarify how many potentially disease causing variants have been identified on exome sequencing after the bioinformatics evaluation and how many could be excluded by segregation analysis within the family*. »

- This information is presented in figure 5A. We found more than 60 000 variants in each patient. After filtering and exclusion of known polymorphisms, heterozygous variants in 5 different genes were shared by the 2 patients. The *CHCHD10* variant only co-segregated with the disease in 8 patients (and was absent in 2 unaffected individuals).

3) « *I would also like to add to the pedigree, which family members were tested on segregation analysis and what the result was, because still the segregation within the family is the major evidence for the pathogenicity of the mutation* ».

- We fully agree with the referee that this information is a major evidence for the pathogenicity of the mutation. The pedigree has been completed. In the first version of the article, we forgot to precise that this mutation was absent in 2 healthy old individuals and a sentence has been added to strengthen this point.
  Page 15 – Lines 4-8 : Segregation analysis showed that the mutation was present in the 8 patients tested and was absent in 2 healthy individuals (IV-14 and IV-16) with normal neurological examination at 79 and 69 years, respectively.

4) « *On Figure 2 how can the authors explain the additional bands with complex V antibodies on BN-PAGE*? »

- This question was also raised by the first referee. As we stated in paragraph 1) secondary to his comments, smaller bands observed with complex V antibodies can be secondary either to an abnormal assembling or to a degradation of the complex.

For Peer Review

5) « *I feel a bit, that all functional studies are aiming to provide evidence for some indirect signs of abnormal fusion/fission and do not answer what the exact function of the CHCHD10 gene is. Although I find it good that the authors determined the localization of this protein in mitochondria* ».

- This comment corresponds to the one of the first referee and novel data are shown in figure 4.

6) « *Mitochondrial fragmentation and network length are quite non-specific findings and may present in different conditions. So I feel that the evidence for the pathogenicity of the mutation is not completely convincing* ».

- Indeed, it is easier to prove the pathogenicity of recessive mutations by complementation leading to phenotypic reversion in patient fibroblasts. We agree that mitochondrial fragmentation is not synonymous with a fusion defect. For example, ROS production during mitochondrial dysfunction leads to mtDNA damage and lipid peroxidation. This process involves membrane damage and changes in the mitochondrial network with fragmented mitochondria, and secondary fusion deficiency. However, mitochondrial fragmentation and cristae alterations observed after CHCHD10 ^{S59L} overexpression replicate the phenotype observed in patient fibroblasts. These results mainly associated with the segregation analysis in this large family but also with the mitochondrial localization of CHCHD10 make difficult to challenge the pathogenicity of the identified variant.

Referee 3

Major comments

1) « *The observation of a FTD-ALS phenotype in a mitochondrial disease is novel and would deserve to be better emphasized and documented, especially:*
- What about the brain MRI of CHCHD10 mutated patients with FTD? FTD is commonly associated with fronto-temporal atrophy.
- Did any of the patients undergo a PET-scan?
- Was there any analysis in the CSF to measure a-beta or Tau levels? »

- In this family, the majority of patients were seen many years ago. We found MRI of 6 patients (III-2, IV-3, IV-11, IV-13, V-2, V-10) and, interestingly, none showed specific abnormality. This point has been added in the text.
Page 5 – Lines 11-13: Brain MRI of patient V-10 was normal and the one of the patient IV-3 showed moderate cortical atrophy. Brain MRI performed in 4 other patients (III-2, IV-11, IV-13, V-2) showed no specific abnormality.
No patient underwent a PET-scan and a-beta or Tau levels were not measured in CSF.

2) « *Abnormal mitochondrial fragmentation can be of multiple origins. The authors try to demonstrate the action of CHCHD10 on mitochondrial fusion by using a mutant of DRP1, which should prevent fission. The fact that the relative fragmentation induced by the CHCHD10 mutant is not modified by the DRP1 mutant rather suggests that the DRP1 mutant does not exert its dominant negative effect as it should. If the DRP mutant were to be active (as claimed by the authors), then the mitochondrial compartment would be filamentous.* »

For Peer Review

- We agree that DRP experiment was not a good approach and it has been replaced, as explained above, by photoactivable GFP assay.

Other comments

1- « *The authors should display the actual values of the respiratory chain analyses performed in muscle as it would help interpreting the amount of mitochondrial deletions* »

.

- We cannot conclude that the RC deficiency that we observed in muscle is directly correlated to mtDNA deletion load. In this family, the situation is the same than the one found in « ADOA plus » phenotype associated with mutations in *MFN2* or *OPA1*. Patients present a RC defect in muscle with mtDNA deletions but they also have mitochondrial dysfunction in fibroblasts in the absence of mtDNA deletions (Amati-Bonneau *et al*., 2008 ; Rouzier *et al.,* 2012).
Mitochondrial diseases are characterized by their tissue specificity and it is likely that CHCHD10 dysfunction has numerous consequences in terms of membrane damage, cristae disorganization, ROS production that all contribute to RC deficiency. That is the reason why, even if mtDNA deletions found in muscle highly contribute to the decrease in RC complexes activity, there is no direct correlation between deletion load and RC defect intensity. As there are a lot of tables and figures in the paper, that are more informative than a supplementary table including all biochemical results in muscle of the 8 patients, we prefered to summarize RC activity data in Table 1.

2- « *CHCHD10 seems to be located in the inter-membrane space whereas mitochondrial DNA stands inside the matrix of the mitochondria. Therefore, how do the authors explain the impact of CHCHD10 mutations on the maintenance of mitochondrial DNA*? »

- In the absence of fusion deficiency, it is not possible to clearly answer to this question. However the link between nucleoids and mitochondrial cristae could be involved in mtDNA instability. A paragraph has been added in the discussion to evoke this possibility.
Page 15 - Lines 4-8 : Mitochondrial DNA instability found in patients carrying the p.Ser59Leu *CHCHD10* mutation cannot be explained by a fusion deficiency. However, mammalian cells contain thousands of copies of mtDNA assembled into hundreds of nucleoids that are closely associated with the inner membrane and often appear to be wrapped around cristae or crista-like inner membrane invaginations (Brown *et al.*, 2011). One cannot exclude that cristae alterations secondary to CHCHD10^{S59L} expression lead to nucleoid structures disorganization and contribute to defect of mtDNA maintenance.

3- « *The interpretation of the respiratory chain analyses performed in the fibroblasts of one patient is not clear. How do the authors explain normal respiration under glucose but abnormal respiration under galactose? Since fibroblasts do not show mitochondrial DNA deletions, does it mean that the mechanism by which the respiration is abnormal in fibroblasts is different from the mechanism in muscle?* »

- This test is routinely performed to explore mitochondrial dysfunction and to characterize the energetic competence of patient cells. During incubation in a glucose-free medium containing galactose, cells are forced to rely predominantly

on oxidative phosphorylation for ATP synthesis, given the low efficiency of this carbon source to feed the glycolytic pathway (Robinson et al., 1992). In cells with mitochondrial dysfunction, this experiment helps to highlight an underlying RC deficiency contrary to control cells, which do not present any defect in galactose medium.
Mitochondrial disorders are characterized by tissue specificity and as we explained above, it is clear that RC defect found in different tissues depends on numerous parameters. Indeed, it is likely that even if mitochondrial dysfunction in muscle and fibroblasts has a common primary origin, the consequences are different and both abnormal respiration and RC activity defect measured in fibroblasts are not secondary to mtDNA deletions.

4- « *Did the authors screen CHCHD10 in other families with FTD-ALS?* »

- This comment was really relevant. We had previously analyzed 32 patients with multiple mtDNA deletions without finding any mutation in *CHCHD10*. Then, we screened a cohort of 21 FTD-ALS families which had been analyzed by exome sequencing. We identified one family with the same pSer59Leu mutation in *CHCHD10* and a result paragraph has been added in the manuscript **(Page 18 - Lines 14-25, Page 19 – Lines 1-10**).
Furthermore, the identification of this second family led us to modify the title and highly improved the impact of the paper.

5- « *The numbers of figures could be reduced*. » We deleted the figure 5. However, we performed numerous additional experiments requested by the 3 referees. So, it was not possible to reduce the number of figures.

For Peer Review

A mitochondrial origin for frontotemporal dementia and amyotrophic lateral sclerosis through *CHCHD10* involvement

*Sylvie Bannwarth,[1,2] *Samira Ait-El-Mkadem,[1,2] Annabelle Chaussenot,[1,2] Emmanuelle C. Genin,[1] Sandra Lacas-Gervais,[3] Konstantina Fragaki,[1,2] Laetitia Berg-Alonso,[1] Yusuke Kageyama,[4] Valérie Serre,[5] David Moore,[6] Annie Verschueren,[7] Cécile Rouzier,[1,2] Isabelle Le Ber,[8,9] Gaëlle Augé,[1,2] Charlotte Cochaud,[2] Françoise Lespinasse,[1] Karine N'Guyen,[10] Anne de Septenville,[8] Alexis Brice, [8] Patrick Yu Wai Man,[6] Hiromi Sesaki, [4] Jean Pouget,[7] Véronique Paquis-Flucklinger,[1,2]

* These authors contributed equally to the study

[1]IRCAN, UMR CNRS 7284/INSERM U1081/UNS, School of Medicine, Nice Sophia-Antipolis University, France
[2]Department of Medical Genetics, National Centre for Mitochondrial Diseases, Nice Teaching Hospital, France
[3]Joint Center for Applied Electron Microscopy, Nice Sophia-Antipolis University, France
[4]Department of Cell Biology, Johns Hopkins University School of Medicine, Baltimore, MD, 21205, USA
[5]UMR7592 CNRS, Jacques Monod Institute, Paris Diderot University, France
[6]Wellcome Trust Centre for Mitochondrial Research, Institute of Genetic Medicine, International Centre for Life, Newcastle University, Newcastle upon Tyne NE1 3BZ, UK
[7]Department of Neurology, Timone Hospital, Marseille Teaching Hospital, France
[8]Sorbonne Université, UPMC Univ Paris 06, UM75, Inserm U1127, Cnrs UMR7225, Institut du Cerveau et de la Moelle épinière (ICM), F-75013 Paris, France.
[9]National Reference Centre on Rare Dementias, AP-HP, Groupe Hospitalier Pitié-Salpêtrière, Paris, France
[10]Department of Medical Genetics, Timone Hospital, Marseille Teaching Hospital, France
[11]Newcastle Eye Centre, Royal Victoria Infirmary, Newcastle upon Tyne, NE1 4LP, UK

Running title: *CHCHD10* and mitochondrial disorder

Key words: *CHCHD10*, mitochondrial DNA instability, mitochondrial disorder, FTD-ALS

Word count : 5886 words

Correspondence to:

Prof. Véronique Paquis-Flucklinger
IRCAN UMR CNRS 7284 / INSERM U1081 / UNS
School of Medicine, 28 av de Valombrose,
06107 Nice cedex 2, France.
Tel: (33) 4 93 37 77 86
Fax: (33) 4 93 37 70 33
e-mail: paquis@hermes.unice.fr

For Peer Review

ABSTRACT

Mitochondrial DNA (mtDNA) instability disorders are responsible for a large clinical spectrum, among which amyotrophic lateral sclerosis-like symptoms and frontotemporal dementia are extremely rare. We report a large family with a late-onset phenotype including motor neuron disease, cognitive decline looking like frontotemporal dementia, cerebellar ataxia and myopathy. In all patients, muscle biopsy showed ragged-red and COX negative fibres with combined respiratory chain deficiency and abnormal assembly of complex V. The multiple mtDNA deletions found in skeletal muscle revealed a mtDNA instability disorder. Patient fibroblasts present with respiratory chain deficiency, mitochondrial ultrastructural alterations and fragmentation of the mitochondrial network. Interestingly, expression of matrix-targeted photoactivable GFP showed that mitochondrial fusion was not inhibited in patient fibroblasts. By whole-exome sequencing (WES), we identified a missense mutation (c.176C>T; p.Ser59Leu) in the *CHCHD10* gene that encodes a coiled-coil helix coiled-coil helix protein, whose function is unknown. We show that CHCHD10 is a mitochondrial protein located in the intermembrane space and enriched at cristae junctions. Overexpression of *CHCHD10* mutant allele in HeLa cells led to fragmentation of the mitochondrial network and ultrastructural major abnormalities including loss, disorganization and dilatation of cristae.

The observation of a frontotemporal dementia-amyotrophic lateral sclerosis (FTD-ALS) phenotype in a mitochondrial disease led us to analyse *CHCHD10* in a cohort of 21 families with pathologically proven FTD-ALS. We identified the same missense p.Ser59Leu mutation in one of these FTD-ALS families. This work opens a novel field to explore the pathogenesis of FTD-ALS clinical spectrum by showing that mitochondrial disease may be at the origin of some of these phenotypes.

For Peer Review

INTRODUCTION

Mitochondrial disorders can result from defects in mitochondrial DNA (mtDNA) or in nuclear genes that encode proteins that are imported in the mitochondria. Last years, a growing list of genes responsible for mtDNA instability has been reported (Copeland, 2012; Ylikallio *et al.,* 2012; Shapira *et al.,* 2012). Mutations in these genes lead either to mitochondrial DNA depletion syndrome (MDS), a devastating mitochondrial disease of childhood associated with a significant reduction of mtDNA copy number, or disorders characterized by accumulation of multiple mtDNA deletions in postmitotic tissues (Suomalainen *et al.,* 2010; Copeland, 2012). Diseases associated with deletions comprise commonly known clinical presentations including progressive external ophtalmoplegia (PEO) and ataxia neuropathy syndromes but also some rares disorders (for review see Copeland, 2012). To date, nuclear genes responsible for mtDNA instability disorders mainly fall into three categories : (i) genes encoding proteins directly involved in mtDNA replication, such as *POLG*, *POLG2* or *TWINKLE*, (ii) genes encoding proteins responsible for the maintenance of mitochondrial nucleotide pool, such as *TP, TK2, DGUOK*… and, (iii) genes encoding membrane proteins involved in mitochondrial dynamics, such as *OPA1* or *MFN2* (Amati-Bonneau *et al.,* 2008; Hudson *et al.,* 2008; Rouzier *et al.,* 2012). This third category was recently individualized. Autosomal dominant optic atrophy (ADOA) is mainly related to mutations in the optic atrophy 1 gene (*OPA1*) which encodes a dynamin-like GTPase involved in the fusion of the inner mitochondrial membrane (Delettre *et al.,* 2000). Mitofusin 2 (Mfn2) is one of the two mitofusin proteins also required for mitochondrial fusion. Mfn1 and Mfn2 are conserved integral outer mitochondrial membrane proteins, each consisting of a large GTPase domain and 2 heptad repeat (HR), or putative coil-coiled domains, all of which face the cytoplasm (Koshiba *et al.,* 2004; Meeusen *et al.,* 2004; Song *et al.,* 2009). *MFN2* mutations are a major cause of primary axonal Charcot-Marie-Tooth

For Peer Review

disease type 2A (CMT2A) (Zuchner *et al.,* 2004), an autosomal dominant neuropathy that impairs motor and sensory neurons with the longest axons resulting in earliest symptoms in distal extremities. A subset of *OPA1* missense mutations have been associated with the "ADOA plus" syndrome and with accumulation of mtDNA deletions in muscle (Amati-Bonneau *et al.,* 2008; Hudson *et al.,* 2008). Complex phenotypes have also been associated with *MFN2* mutations. Recently, we reported a large family with optic atrophy beginning in early childhood, associated with axonal neuropathy and mitochondrial myopathy with mtDNA deletions in adult life. The clinical presentation looks like the "ADOA plus" phenotype linked to *OPA1* mutations but is associated with a novel *MFN2* missense mutation, thus confirming the link between mtDNA stability and mitochondrial fusion (Rouzier *et al.,* 2012).

Here, we report the involvement of a novel gene responsible for "mitochondrial DNA breakage" syndrome and frontotemporal lobe dementia-amyotrophic lateral sclerosis (FTD-ALS) through 2 families from French and Spanish origin. The responsible gene, *CHCHD10,* encodes a coiled-coil helix coiled-coil helix protein whose function is unknown. However, CHCHD10 belongs to a family of mitochondrial proteins located in the intermembrane space, some of which interact with OPA1 and are involved in cristae integrity and mitochondrial fusion (Darshi *et al.,* 2011; An *et al., 2012*).

PATIENTS AND METHODS

Patients

The pedigree of the first family of French origin is shown in Fig. 1. All clinical data are summarized in table 1. Blood and tissue samples were obtained after patients had given informed consent. The index case was a 67-year-old woman (IV-6), who developed a cerebellar ataxia at 50 years of age, associated with progressive bulbar syndrome, dementia

For Peer Review

and sensorineural deafness. Clinical examination showed cerebellar ataxia, Babinski sign, areflexia and bulbar palsy with dysarthria and dysphagia. Neuropsychological tests revealed a frontal lobe syndrome. Laboratory investigations showed normal lactate concentrations (1.6 mmol/l, normal <2.1 mmol /l). She died at 67 years of age.

The age of onset of the 7 other patients who underwent a muscle biopsy was between 49 and 65 year-old. Three patients presented a motor neuron disease (MND), 2 a cerebellar ataxia and the last two had a MND and a cerebellar ataxia, like the index case. All developed cognitive disorders with mainly a frontal lobe syndrome, except patient V-2 who died at 51 year-old. Neuropsychological evaluation of patient IV-3 showed severe impairment in episodic memory, attention, verbal fluency and executive functions with behavioral changes corresponding to frontal dementia. Brain MRI of patient V-10 was normal and the one of the patient IV-3 showed moderate cortical atrophy. Brain MRI performed in 4 other patients (III-2, IV-11, IV-13, V-2) showed no specific abnormality. Proximal weakness was observed in 4 individuals (IV-3, IV-11, IV-13 and IV-15) with bilateral ptosis and facial paresis in patient IV-15. Electromyography excluded peripheral neuropathy with normal test (V-10), chronic neurogenic changes suggesting a lower motor neuron disease (IV-15) or myopathic abnormalities only (IV-3). Patients IV-3 and V-10 are still alive, all others died after more than 10 years of evolution.

Other affected individuals had no muscle biopsy (I-1, II-1, II-2, II-6, III-1, III-4, III-5, III-6, III-7, III-8 and IV-9). They presented dementia, progressive bulbar syndrome with dysarthria and dysphagia, and became bedridden.

Muscle histopathology and ultrastructure

Muscle samples were frozen in cooled isopentane and stored in liquid nitrogen for histological and histoenzymatic analysis including Gomori modified trichrome staining, cytochrome *c* oxydase (COX) activity, succinate dehydrogenase (SDH) activity and double

For Peer Review

COX/SDH staining according to standard protocols. A fragment of muscle was also fixed in 2% glutaraldehyde and processed for ultrastructural analysis by electron microscopy.

OXPHOS spectrophotometric measurements

Enzymatic spectrophotometric measurements of the OXPHOS respiratory chain complexes and citrate synthase were performed at 37°C on muscle crude homogenates and fibroblasts according to standard procedures (Rustin *et al.,* 1994).

Polarographic study

Polarographic studies on fibroblasts of intact cell respiration and digitonin (0.004%)-permeabilized cells mitochondrial substrate oxidation were carried out as previously described (Rustin *et al.,* 1994).

Blue native gel electrophoresis (BN-PAGE) and immunoblotting

15 µg of muscle mitochondrial respiratory complexes, obtained by solubilisation in a solution of 1.5 M aminocaproic acid (Sigma-Aldrich), 75 mM BIS-TRIS (Sigma-Aldrich) and 4% dodecyl-β-D-maltoside (Sigma-Aldrich), were separated by BN-PAGE on a 4–13% acrylamide gradient gel (Schägger *et al.,* 2001). Then they were electroblotted onto a PVDF membrane, prior to sequential incubation with specific antibodies directed against GRIM19 subunit of complex I, SDHA subunit of complex II, UQCRC2 subunit of complex III, MTCO1 subunit of complex IV and ATP5A subunit of complex V (Mitosciences) allowing to verify that samples were equally loaded between patients and controls.

Protein measurement

Proteins were measured according to Bradford microassay (Bradford, 1976).

mtDNA molecular analysis

Total DNA was extracted using standard phenol chloroform procedure. Long-range PCR and Southern blot analysis were performed as previously described (Paul *et al.,* 1996; Moraes *et al.,* 1996). mtDNA quantification in muscle was performed by real-time quantitative PCR as

For Peer Review

described by Rouzier *et al*., 2010. Primer sequences and PCR conditions are available on request.

Sequencing of nuclear genes

The coding regions of *POLG* (NM_002693.2), *SLC25A4* (ANT1*)* (NM_001151.3) and *PEO1* (Twinkle*)* (NM_021830.4) genes were sequenced as previously described (Naimi *et al.,* 2006). PCR products were purified with Illustra ExoStar enzyme (GE Healthcare), processed with an ABI PRISM® dRhodamine Terminator Cycle Sequencing Ready Reaction kit (Applied Biosystems) and analyzed on an ABI 3130XL automated sequencer (Applied Biosystems).

Cell culture

Skin punches were obtained from patient V-10 after informed consent. Primary fibroblast cultures were established using standard procedures in RPMI supplemented with 10% Fetal Bovine Serum (FBS), 45µg/ml uridine and 275µg/ml sodium pyruvate. Cultures were incubated at 37°C with 5% CO_2. For galactose conditions, medium was replaced 24h before experiments by glucose-free medium containing 5mM galactose and 5mM pyruvate (Zanna *et al.,* 2008).

HeLa cells were maintained in DMEM supplemented with penicillin (100U/ml)/streptomycin (0.1mg/ml), 10% fetal calf serum (FCS), at 37°C in a humidified atmosphere with 5% CO_2 in air. For transient transfections, HeLa cells were transfected using Lipofectamine 2000 (Invitrogen) according to the manufacturer's instructions.

Mitochondrial network analysis

For mitochondrial staining, cells were incubated in a 100nM solution of MitoTracker red (Invitrogen) for 15 min, medium was replaced by HeLa cells culture medium incubated 2 h at 37°C and washed in PBS. The samples were fixed with paraformaldehyde (PFA) 4% (Electron Microscopy Sciences), washed with PBS, and mounted on glass slides using

For Peer Review

Prolong Gold Antifade Reagent (Molecular Probes). For immunostaining, cells were fixed with 4% PFA, washed five times with PBS and permeabilised with 2% Triton X-100. After PBS washing, coverslips were incubated with 5% BSA (Bovin Serum Albumin) for 30 min at room temperature before adding mouse anti-FlagM2 (Agilent Technologies) (1/2000 antibody diluted with PBS-BSA 5%), mouse anti-HA (Cell Signaling) (1/100 antibody diluted with PBS-BSA 5%) or rabbit anti-FlagM2 (Cell Signaling) (1/800 antibody diluted with PBS-BSA 5%). The samples were incubated at room temperature for 1h, PBS washed, and then incubated with fluorescent secondary antibody goat anti-mouse Alexa 488 (Life Technologies) (1/1000 antibody diluted with PBS-BSA 1%) or antibody goat anti-rabbit Alexa 647 (Life Technologies) (1/1000 antibody diluted with PBS-BSA 1%) for 1 hour at room temperature. The coverslips were washed five times with PBS, mounted on glass slides using Prolong Gold Antifade Reagent (Molecular Probes) and analyzed using a Zeiss LSM510 meta confocal laser-scanning microscope.

The images were deconvolved with Huygens Essential Software™ (Scientific Volume Imaging) using a theoretically calculated point spread function (PSF) for each of the dyes. All selected images were iteratively deconvolved with a maximum iterations scored 40 and a quality threshold at 0.05. The deconvolved images were used for quantitative mitochondrial network analysis with Huygens Essentiel Software™ with the following standardised set of parameters: threshold = 25% and seed = 0% for each cell types and garbage = 5 or 10 for HeLa cells and fibroblasts respectively. The quantitative data were further analysed in Microsoft Excel and GraphPad Prism 5 (GraphPad Software). Mitochondrial network length was quantified for 35 randomly-selected individual cells.

Data are represented as mean ± S.E.M. Statistical analyses were performed by Student's unpaired t-test using GraphPad Prism 5 (GraphPad Software).

For Peer Review

Exome sequencing

Genomic DNA was extracted from blood and 3µg were fragmented by sonication. Exome targets were enriched with the SureSelect Human All Exon v4+UTR – 70 Mb Kit (Agilent technologies) and sequenced on the Illumina HiSEQ 2000 platform (Illumina). Raw image files were processed by the IlluminaReal Time Analysis pipeline for base calling and generating the read sets. The bioinfomatics analysis of sequencing data was based on the Illumina CASAVA pipeline (v1.8). CASAVA performs alignment of the 2x75 bp paired-end sequence reads to the hg19 reference genome, calls the SNPs based on the allele calls and read depth, and detects variants (SNPs &Indels). The alignment algorithm used was ELANDv2e. Only the positions included in the bait coordinates were conserved. The web application ERIS (Integragen) was used for data visualization and prioritization of variants.

For mutation validation and segregation analysis, a part of *CHCHD10* (NM_213720.1) spanning the mutation site in exon 2 was amplified with the following primers: 5'-TCGGGCCAGCCGGGGCTC-3' (forward) and 5'-GGAAGCCTGCCTCTAAGTGA-3' (reverse). Purification and sequencing of PCR products were performed as described above.

Homology modelling of human CHCHD10

Using the threading program PHYRE2 (Kelley *et al.,* 2009), 142 residues of CHCHD10 (Met1 to Pro142) were modeled using CHCHD5 as template (PDB ID: 2LQL). Swiss-Pdb Viewer 3.7 (http://www.expasy.org/spdbv) was used to analyze the structural insight into CHCHD10 mutation and visualize the structure.

Plasmid constructions

The human full-length *CHCHD10* cDNA was amplified by RT-PCR from total RNA of patient fibroblasts by using Transcription First strand cDNA synthesis kit (Roche) and Taq PCRx DNA polymerase (Invitrogen).

For Peer Review

We used the following primers: 5'-GGATCCACCGCCGCCACCATG-3' (forward) and 5'-CTCGAGGGGCAGGGAGCTCAG-3' (reverse) containing *Bam*HI and *Xho*I restriction sites, respectively. Restriction-digested PCR products were cloned into pCMV-3tag-3A to generate Flag-tagged CHCHD10. Sequencing of the clones obtained led to the identification of plasmids coding for wild-type ($CHCHD10^{WT}$) and mutant ($CHCHD10^{S59L}$) cDNAs.

Western blotting

5-25 µg of total protein extracts were separated on acrylamide-SDS gels and transferred to PVDF membranes (Millipore, Saint-Quentin). Specific proteins were detected by using mouse anti-Mfn2 (1/2000, Abcam, #ab56889), anti-VDAC (1/2000, Millipore, #MABN504), anti-Flag M2 (1/2000, Agilent Technologies, #200412), anti-PCNA (1/5000, BD Biosciences, #610664), rabbit polyclonal anti-mitofilin (1/2000; Proteintech #10179-1-AP), anti-GAPDH (1/20000, Abcam #ab9485), anti-β tubulin (1/10000, Sigma-Aldrich, #T4026), anti-SMAC (1/4000, Abcam #ab8114), anti-TOM 20 (1/5000, BD Biosciences, #612278), anti-CHCHD10 (1/500, Sigma-Aldrich #HPA003440) and goat polyclonal anti-Hsp60 (1/4000, Santa Cruz, #sc-1052) antibodies. Anti-mouse, anti-rabbit or anti-goat secondary antibody (Dako) was used at 1/10000 and signals were detected using a chemiluminescence system (Immobilon Western HRP Chemilumiscent substrates, Millipore). Human multiple tissue blot was used as described by the manufacturer (G-Biosciences).

Isolation of mitochondria and mitoplast preparation

Mitochondria were isolated from HeLa transfected cells using Q-Proteome mitochondria isolation kit (Qiagen) as described by the manufacturer. Mitochondria were treated with Proteinase K (Invitrogen) in the presence or absence of 0.2% TritonX-100 exactly as described in Bannwarth *et al.,* 2012. To prepare the mitoplasts, we used a digitonin treatment. Briefly, purified mitochondria were suspended in suspension buffer (250 mM sucrose, 1mM EDTA, 20mM HEPES-NaOH, pH7.4). Mitochondria were treated with digitonin (2mg/ml)

For Peer Review

15 min at room temperature. The resulting mitoplasts were treated 10 min at room temperature with Proteinase K (100ng/µl). Proteolysis was halted by the addition of 10mM PMSF (Sigma-Aldrich) for 15 min on ice. Laemmli sample buffer was added directly to samples, boiled and loaded on SDS-PAGE.

Alkali extraction of intact mitochondria

Alkali extraction was performed as previously described (Bannwarth *et al.,* 2012). Briefly, intact isolated mitochondria (25µg) were treated with 0.1M Na_2CO_3 (pH 11.5) for 30 min on ice, and then centrifuged at 16,000g for 15 min at 4°C. Supernatants were retained and pellets were washed once and then resuspended in an equivalent volume of homogenization buffer (250mM sucrose, 1mM EDTA, 20mM Hepes-NaOH pH7.4, plus protease inhibitor). Equivalent volumes were analyzed by immunoblot.

Immunoelectron microscopy

Cells were fixed with 2% paraformaldehyde, 0.2% glutaraldehyde in 0.1 M phosphate buffer (pH 7.4) for 2 hr and were processed for ultracryomicrotomy according to a slightly modified Tokuyasu method (Tokuyasu, 1973). In brief, cell suspension was spun down in 10% gelatin. After immersion in 2.3 M sucrose (in [pH 7.4], 0.1 M PB) overnight at 4°C, the samples were rapidly frozen in liquid nitrogen. Ultrathin (70 nm thick) cryosections were prepared with an ultracryomicrotome (Leica EMFCS) and mounted on formvar-coated nickel grids (Electron Microscopy Sciences). Immunostainings were processed with an automated immunogold labeling system Leica EM IGL as following: the grids were incubated successively in PBS containing 50 mM NH4Cl (5 min twice), PBS containing 1% BSA (5 min twice), PBS containing rabbit anti-CHCHD10 (Sigma-Aldrich) or anti-Hsp60 (Abcam, #ab46798) antibody in 1% BSA for 1 h, PBS containing 0.1% BSA (5 min 3 times), PBS containing 1% BSA and 10 nm colloidal gold conjugated protein AG (CMC), PBS containing 0.1% BSA for

For Peer Review

5 min, PBS for 5 min twice. Lastly, the samples were fixed for 10 min with 1% glutaraldehyde, rinsed in distilled water and were contrasted with a mixture of 1.8% methylcellulose and 0.3% uranyl acetate on ice. After having been dried in air, sections were examined under a JEOL 1400 transmission electron microscope.

Mitochondrial fusion assay

Mitochondrial fusion was examined using mitochondria-targeted photoactivatable GFP (mitoPAGFP), as described (Karbowski *et al.*, 2004). The matrix-targeted presequence from Su9 (Wakabayashi *et al.*, 2009) was fused to the N-terminus of photoactivatable GFP (Addgene #11910) and cloned into the lentiviral vector pHR-SIN (Kim *et al.*, 2011). Fibroblasts were infected with lentiviral particles carrying mitoPAGFP. 30 min before observation, fibroblasts were stained with 7 nM tetramethylrhodamine ethyl ester to visualize mitochondria. mitoPAGFP was photoactivated by 405-nm light (30% power, three times) in a small region (30 x 30 pixels) using a Zeiss 780 LSM confocal microscope with an environmentally controlled chamber. Images were taken at 15-min intervals for 60 min. Fluorescence intensity of mitoPAGFP was quantified using NIH Image J.

RESULTS

Mitochondrial myopathy with multiple mtDNA deletions in patients

Muscle biopsy was performed in 8 patients after informed consent (III-2, IV-3, IV-6, IV-11, IV-13, IV-15, V-2, V-10) (Fig.1). Muscle analysis of the index case (IV-6) showed typical features of mitochondrial myopathy including intracellular lipid accumulation with COX-negative and ragged-red fibres (RRF) (30%) (Fig.2A-B). Electron microscopy showed altered morphology of mitochondria and cristae organization with paracristalline inclusions (Fig.2C). Similar findings with numerous RRF and COX-deficient fibres were found in all patients tested. Spectrophotometric analysis showed a combined respiratory chain deficiency in most

For Peer Review

patients (Table 1). BN-PAGE assay of patients IV-3 and V-2 revealed smaller bands with antibody against complex V corresponding to assembly defect or increased instability (Fig.2D). All patients carried multiple mtDNA deletions in muscle identified by both long range PCR (not shown) and Southern blot analysis (Fig.2E). The determination of relative mtDNA copy number was performed by real-time quantitative PCR without finding any depletion (not shown).

Respiratory chain deficiency, abnormal mitochondrial network and mitochondrial ultrastructural alterations in patient fibroblasts

Spectrophotometric analysis of fibroblasts from patient V-10 cultivated in glucose medium revealed no respiratory chain deficiency and polarographic analysis showed normal oxygen consumption and mitochondrial substrate oxidation (Table 2A, 2C). In a glucose-free medium containing galactose, cells are forced to rely predominantly on OXPHOS for ATP production because the carbon source feeds the glycolytic pathway with a low efficiency. In galactose medium, spectrophotometric analysis revealed a multiple RC deficiency in patient fibroblasts and polarographic analysis showed a decrease of oxygen consumption, glutamate/malate and succinate (Table 2B, 2D). BN-PAGE analysis of patient fibroblasts revealed no abnormality including complex V (not shown), the activity of which was normal by spectrophotometry. Multiple mtDNA deletions were not observed and the determination of relative mtDNA copy number was performed by real-time quantitative PCR without finding any depletion (not shown).

We also compared the mitochondrial morphology of fibroblasts from patient V-10 with that obtained from control fibroblasts. After staining with Mitotracker and examination by confocal microscopy, control fibroblasts in glucose medium displayed a typical filamentous interconnected network. Patient fibroblasts presented with a fragmentation of the

For Peer Review

mitochondrial network and less connected mitochondria (Fig.3A-B). We obtained the same results in galactose medium (not shown).

We then performed ultrastructural analysis of patient fibroblasts. Typical mitochondria of control cells had numerous, thin, well□defined cristae, running perpendicularly to the mitochondrial longitudinal axis, and with a regular pattern of parallel organization (Fig.3C). They represented 90% of the mitochondrial profiles seen in two independent, genotype-blind, analyses of control cells. In patient cells, they represented 35% of the mitochondrial profiles. Completely disorganized mitochondria with sparse or absent cristae without recognizable parallel orientation were only observed in patient fibroblasts (18%) (Fig.3D). Less disorganized mitochondria represented 47% of the mitochondrial pattern in patient cells and 10% in control cells (Fig.3E).

No mitochondrial fusion defect in patient fibroblasts

The fragmentation of mitochondrial network observed in patient fibroblasts can be of different origins including a fusion deficiency. Furthermore, genes like *MFN2* or *OPA1* involved in mitochondrial fusion are responsible for complex neurological phenotypes associated with mtDNA deletions. To examine mitochondrial fusion, we expressed matrix-targeted photoactivatable GFP in control and patient fibroblasts (Karbowski *et al.*, 2004). After photoactivation of mitoPAGFP in a portion of mitochondria, we monitored mixing of the fluorescent matrix marker. We found that the fluorescence intensity of mitoPAGFP similarly decreased for 60 min in both fibroblasts, suggesting that mitochondrial fusion is not inhibited in patient fibroblasts (Fig.4).

Identification of a missense mutation in the *CHCHD10* gene by exome sequencing

Analysis of genes involved in multiple mtDNA deletions with a compatible phenotype (*POLG*, *SLC25A4*, *PEO1*) revealed no mutation. To identify the causative gene, we sequenced the exome of patients IV-11 and V-10. The procedure yielded 9.8 and 12.4 Gb of

mappable sequence and after alignment to the hg19 reference genome, the average depth was ~70x and ~91x, respectively. From the 62 252 and 63 036 identified SNPs in patients IV-11 and V-10 respectively, the pathogenic variant was identified by the following scheme: (1) Selection of heterozygous variants shared by the 2 patients, (2) Exclusion of polymorphic variants present in dbSNP132, EVS (Exome Variant Server), HapMap, 1000 Genome databases and in-house control exomes (3) Segregation analysis within the family. This filtering led us to identify a single heterozygous missense mutation (c.176C>T; p.Ser59Leu) in exon 2 of *CHCHD10* that was present in the 8 patients tested and was absent in 2 healthy individuals (IV-14 and IV-16) with normal neurological examination at 79 and 69 years, respectively (Fig.5A-B). This gene encodes the coiled-coil helix coiled-coil helix domain-containing protein 10 whose function is unknown. However, the C-terminal CHCH domain is primarily seen in mitochondrial proteins and was known to be involved in the protein import and metal binding in the intermembrane space (Banci *et al.,* 2009). The mutation changes a highly conserved serine into a leucine and was not present in 200 ethnically and geographically matched control alleles (Fig.5C). *In silico* study by PolyPhen-2 (http://genetics.bwh.harvard.edu/pph2/), SIFT (http://sift.jcvi.org/) and Mutation Taster (http://www.mutationtaster.org/) predicted this variant to be probably damaging.

The CHCH domain of CHCHD10 is characterized by a CX_9C motif. Although all CX_9C proteins presumably preserve a disulfide bonded α-hairpin conformation, they have a large range of sequence lengths and a very low degree of sequence similarity both within or specific organism and the orthologs of different species (Longen *et al.,* 2009; Cavallo *et al.,* 2010). Therefore, these features do not allow to easily predict accurate structural models for this protein family. Recently, Banci *et al*. have structurally characterized two members of them, CHCHD5 and CHCHD7, in their fully oxidized states (Banci *et al.,* 2012). Using the same program, 142 residues of CHCHD10 (Met1 to Pro142) were modeled using CHCHD5

For Peer Review

as template (PDB ID: 2LQL). Swiss-Pdb Viewer 3.7 (http://www.expasy.org/spdbv) was used to analyze the structural insight into CHCHD10 mutation and visualize the structure. The modeling of CHCHD10 shows (i) a non-structured N-terminal region, (ii) a highly hydrophobic helix (Gly43 to Ala 68) which may be typically an interface of interaction with an interacting protein, (iii) and the CHCH domain near the C-terminal region characterized by a CX_9C motif (Fig.5D). The four cysteine residues (102, 112, 122 and 132) of the CHCH domain are involved in two disulfide bonds. The p.Ser59 is located in the hydrophobic N-terminal α-helix, and as the few other polar residues of this helix, it may intervene in hydrogen bonds to stabilize CHCHD10 interaction with another protein. Thus, the p.Ser59Leu mutation could possibly alter protein-protein interactions.

To investigate whether the p.Ser59Leu mutation has an effect on the expression of CHCHD10, we analysed CHCHD10 level in muscle of patients by western blotting. We used GAPDH and the mitochondrial SMAC protein as controls for quantitation. Normalization showed no significant reduction of CHCHD10 expression in patient muscles compared to control (not shown).

CHCHD10 is a mitochondrial protein located in the intermembrane space

First, we looked at the expression of CHCHD10 in human tissues by western blot. The protein is ubiquitous and highly expressed in organs with a high mitochondria content like the heart or liver (Fig.6A). Confocal microscopic analysis then showed a colocalization, in HeLa cells, of endogenous CHCHD10 with MitoTracker, a dye that accumulates specifically in mitochondria (Fig.6B). To analyze submitochondrial localization of CHCHD10, mitochondria isolated from HeLa cells were treated with proteinase K. Proteins inside mitochondria are protected from protease digestion. As shown in Figure 6C, CHCHD10 was resistant to treatment with proteinase K indicating that the protein is present inside mitochondria. As expected, the TOM20 protein (outer mitochondrial membrane) was digested by proteinase K

For Peer Review

while SMAC (intermembrane space) was resistant to protease digestion. Analysis of the mitochondrial preparations for PCNA and GAPDH confirmed the absence of nuclear and cytosolic contaminations, respectively. When mitochondria were subjected to alkali extraction, peripheral membrane proteins were recovered in the supernatant, while integral membrane proteins were found in the membrane-containing pellet fractions (Fig.6D). As expected, the outer membrane integral protein VDAC was primarily recovered in the pellet following extraction while SMAC was recovered in the supernatant. CHCHD10 was distributed in the supernatant indicating that it was located in the soluble fraction. Last, to discriminate between intermembrane space or matrix localization, mitochondria were treated with digitonin to open the inner membrane space. In the resulting mitoplasts, CHCHD10 was degraded by proteinase K like MFN2 (outer mitochondrial membrane), SMAC (intermembrane space) and mitofilin, an inner mitochondrial membrane protein mainly facing the intermembrane space, while Hsp60, which is located in the mitochondrial matrix, was protected against protease digestion (Fig.6E). All these results suggest that CHCHD10 is an intermembrane space protein.

CHCHD10 is enriched at cristae junctions

We performed immunogold labeling of chemically fixed cryosectioned HeLa cells (Fig.7A). The sections were labeled with a primary antibody against CHCHD10, followed by a secondary gold conjugate. For quantitative analysis, we determined the location of each gold particle (n = 229) with respect to the inner boundary membrane and the closest cristae membrane and plotted its respective localization in a model (Fig.7B). We found that the majority of mitochondrial gold particles were enriched in the vicinity of cristae junctions as reported previously for mitofilin, a major component of the MINOS complex (Jans *et al.,* 2013). We performed the same experiment with a primary antibody against Hsp60, a protein highly expressed in the matrix, as a control (Fig. 7C-D).

For Peer Review

Expression of CHCHD10 mutant leads to fragmentation of the mitochondrial network and to defect in cristae maintenance

To confirm the role of the p.Ser59Leu mutation, we analyzed the effects of overexpression of the pathogenic allele on mitochondrial network. HeLa cells were transiently transfected with the empty vector, the wild-type allele or the pathological allele. After transfection, HeLa cells produced equivalent amounts of wild-type and mutant CHCHD10 (Fig.8A). Mitochondrial network morphology and CHCHD10 labeling were next assessed using Mitotracker red and CHCHD10 antibodies, respectively. Forty eight hours after transfection with either empty vector or the wild-type allele, Mitotracker revealed a filamentous network. Overexpression of mutant CHCHD10^{S59L} altered mitochondrial morphology in transfected cells with a significant fragmentation of the network (Fig.8B-C). We also looked at the mitochondrial morphology by electron microscopy. Contrary to overexpression of either empty vector or the wild-type allele, overexpression of the CHCHD10^{S59L} mutant led to major abnormalities including loss, desorganization or dilation of cristae. Matrix condensation was also observed in numerous mitochondria (Fig.9A-D).

Involvement of the same *CHCHD10* mutation in an FTD-ALS family

The observation of a FTD-ALS phenotype in a mitochondrial disease led us to analyze *CHCHD10* variants in a cohort of 21 FTD-ALS families previously tested by exome sequencing. We identified the heterozygous c.176C>T (p.Ser59Leu) mutation in a patient whose family is originally from Catalonia (Spain). This man developed walking difficulties at 57 years of age. Progressively, he presented a pseudo-bulbar syndrome with dysarthria and dysphagia. Electromyography confirmed motor neuron involvement with symmetrical denervation predominent in muscles of the face but also in muscles of upper and lower limbs. Motor and sensory conduction velocities were normal. The patient also had cognitive impairment and behavioural changes suggesting a frontotemporal dementia.

For Peer Review

Neuropsychological testing revealed a frontal lobe dysfunction, notably impairment of conceptualization, perseverative behaviours and paraphasia with relative preservation of memory. Brain MRI showed mild bilateral frontal atrophy. Parkinsonian signs were also present with akinesia, rigidity and gait disorders and a UPDRS scale at 10. In addition, the patient presented bilateral sensorineural hypoacousia and a muscular fatigability. A total loss of autonomy was observed after 8 years of evolution, then he was loss sight. The elder sister and one brother of the index case presented ALS with predominant bulbar features and died after 4 years of evolution. Their father developed a neurological disease with progressive walking and speaking difficulties at 61 years of age leading to death 3 years later. No patient had a muscle biopsy. The presence of the mutation was confirmed by Sanger method in the index case but the absence of DNA samples from other family members did not allow to perform segregation analysis.

DISCUSSION

In this study, we first identified a new gene involved in mtDNA instability disease. We describe a large family in which affected individuals carry a missense mutation in the *CHCHD10* gene. The clinical phenotype associated with this *CHCHD10* mutation is unusual because patients developed a late-onset disease, which begins around fifty, with highly variable clinical presentations. Affected individuals presented with either isolated or associated symptoms including ataxia, dementia and ALS-like presentation; the only element common to all patients being the presence of a mitochondrial myopathy with numerous ragged-red and COX-negative fibers associated with multiple mtDNA deletions. None of the affected individuals presented with an external ophtalmoplegia. A patient only (IV-15) presented with a ptosis associated with facial palsy, probably due to motor neuron disease. In this family, the phenotype is really particular compared to those reported in mtDNA

For Peer Review

instability disorders. The course of the disease was highly variable, ranging from one to more than 15 years of evolution before death. However, it was more severe than the PEO (Progressive External Ophtalmoplegia) phenotypes classically observed in pedigrees with autosomal dominant transmission of multiple mtDNA deletions (Copeland, 2012). Cerebellar ataxia is exceptionnally observed in the absence of PEO in mtDNA instability disease, except in MIRAS or MSCAE phenotypes (Copeland, 2012), secondary to *POLG* mutations, or in IOSCA (Hakonen *et al.,* 2007), secondary to *TWINKLE* mutations. MND with ALS-like symptoms is even rarer with exceptional cases associated with *POLG*, *TK2* or *DGUOK* mutations (Ronchi *et al.,* 2012). The cognitive impairment observed in our family looks like frontotemporal dementia usually observed in ALS patients. This observation led us to analyse *CHCHD10* in FTD-ALS families with a dominant mode of transmission and to identify the same missense p.Ser59Leu mutation in one of these families. FTD-ALS is a genetically heterogeneous disorder and a hexanucleotide repeat expansion in a noncoding region of the chromosome 9 open reading frame 72 (*C9ORF72*) gene, the function of which is unknown, has been recently identified as a common cause of FTD-ALS (DeJesus-Hernandez *et al.*, 2001; Renton *et al.*, 2011). Patients with a *C9ORF72* expansion present with FTD, ALS, or both. Parkinsonism is common and the phenotype of our second family was highly evocative of a *C9ORF72* expansion. However, *C9ORF72* screening and the analysis of other candidate genes for ALS and FTD were negative in this family (*TARDBP, FUS/TLS, SOD1, VCP, CHMP2B, ANG, SQSTM1, UBQLN2, PFN1*). No patient had a muscle biopsy but it is likely that sensorineural hypoacousia and muscle weakness observed in the index case were related to mitochondrial dysfunction. Our study clearly shows that *CHCHD10* is a novel gene responsible for ALS-FTD clinical spectrum, which raises the intriguing prospect of an underlying mitochondrial basis for this group of disorders.

For Peer Review

The function of CHCHD10 is unknown. However, it belongs to a family of mitochondrial proteins characterized by conserved CX_nX motifs (Banci *et al.,* 2009) and it is expected to be involved in oxidative phosphorylation (Martherus *et al.*, 2010). These proteins are incorporated into the intermembrane space and are then trapped through a redox-dependent protein machinery *via* the intermembrane space protein Mia 40 (CHCHD4) (Stojanovski *et al.,* 2012). CHCHD3 is a member of this family predominantly localized to the inner membrane, facing toward the intermembrane space (Darshi *et al.,* 2012). It is part of the large protein complex called as MINOS and plays a role in maintening mitochondrial function and cristae integrity (Darshi *et al.,* 2011; van der Laan *et al.,* 2012). OPA1 has been shown to be involved in regulating cristae remodeling independently of its role in mitochondrial fusion (Frezza *et al.,* 2006). CHCHD3 interacts both with OPA1 and mitofilin suggesting that it is a scaffolding protein that stabilizes complexes involved in maintening cristae architecture (Darshi *et al.,* 2011). Another member of this family, CHCM1/CHCHD6, is critical for maintening the cristae morphology, ATP production and oxygen consumption. It has the same localization than CHCHD3 and strongly interacts with mitofilin (An *et al.,* 2012). Here, we show that CHCHD10 is a mitochondrial protein, located in the intermembrane space. Unlike CHCHD3 and CHCM1/CHCHD6, which are inner membrane-associated proteins, CHCHD10 is a soluble protein. By electron microscopy, we also show that it is enriched at cristae junctions, like mitofilin, suggesting that it could be another actor in maintening cristae morphology. The cristae alterations found both in patient fibroblasts and HeLa cells overexpressing CHCHD10^{S59L} mutant are also in favor of this hypothesis. There is a strong evidence that the mitochondrial F_1F_0-ATP synthase, apart from its enzymatic activity, plays a major role in determining the structure of cristae (Zick *et al.,* 2009). The regular arrangement of this highly abundant protein complex might serve as a kind of backbone stabilizing tubular cristae structures. On the contrary, we could ask whether the

For Peer Review

abnormal pattern observed for F_1F_0-ATP synthase by BN-PAGE analysis in the muscle of patients is not secondary to an abnormal organization of cristae linked to the p.Ser59Leu mutation. Furthermore, this mutation leads to a respiratory chain deficiency both in muscle and fibroblasts of patients suggesting that CHCHD10 is critical for maintening ATP production and oxygen consumption. It has been shown that cristae shape regulates respiratory chain supercomplexes stability and assembly with an impact on mitochondrial respiratory efficiency, thus suggesting that shape of biological membranes can influence membrane protein complexes (Cogliati *et al.,* 2013). Further experiments will be necessary to determine whether these effects of CHCHD10 mutant are linked to destabilization of cristae morphology.

Down-regulation of both *CHCHD3* and *CHCM1/CHCHD6* in HeLa cells resulted in fragmentation and clustering of the mitochondrial network (Darshi *et al.,* 2011; An *et al.,* 2012). This could indicate either increased fission or decreased fusion in knock-out cells. Studies with the dominant negative mutant of Drp1, $DRP1^{K38A}$, which blocks fission, suggested that the mitochondria in CHCHD3 knock-out cells have impaired fusion activity (Darshi *et al.,* 2011). Fibroblasts of patients carrying the *CHCHD10* mutated allele presented a fragmentation of the mitochondrial network and less connected mitochondria. However, a direct assay with a photoactivable mitochondrial form of GFP did not find a mitochondrial fusion defect in patient fibroblasts. The accumulation of mtDNA deletions in skeletal muscle can be secondary to an increase in mtDNA damage, a defect in mtDNA repair and/or a failure to clear mitochondria with damaged DNA (Chen and Chan, 2010). Recently, we have shown that fibroblasts bearing a *MFN2* mutation, responsible for optic atrophy 'plus' phenotype with mtDNA multiple deletions, have a lower capacity to repair stress-induced mtDNA lesions compared to control cells (Rouzier *et al.,* 2012). It is likely that the defect in mtDNA repair

For Peer Review

that we observed is due to defective fusion that leads to a variability in repair protein content across the mitochondrial population, thus contributing to mtDNA instability. Mitochondrial DNA instability found in patients carrying the p.Ser59Leu *CHCHD10* mutation cannot be explained by a fusion deficiency. However, mammalian cells contain thousands of copies of mtDNA assembled into hundreds of nucleoids that are closely associated with the inner membrane and often appear to be wrapped around cristae or crista-like inner membrane invaginations (Brown *et al.*, 2011). One cannot exclude that cristae alterations secondary to CHCHD10^{S59L} expression lead to nucleoid structure disorganization and contribute to defect of mtDNA maintenance.

In conclusion, our study has provided strong supporting evidence that the CHCHD10 protein plays a role in the maintenance of mitochondrial cristae morphology and mtDNA stability. Additonal work will be needed to clarify the pathogenic mechanisms linking *CHCHD10* mutations with these downstream deleterious consequences and ultimately, the observed neurodegenerative phenotype. Moreover, this work opens a novel field to explore the pathogenesis of FTD-ALS clinical spectrum by showing that mitochondrial disease may be at the origin of some of these phenotypes. The analysis of *CHCHD10* also needs to be performed in patients presenting with ALS or FTD in both sporadic and familial cases.

ACKNOWLEDGEMENTS

We acknowledge Pasteur-IRCAN Cellular and Molecular Imaging platform (PICMI). We also acknowledge Pr François Tison (CHU Bordeaux), Cyril Goizet (CHU Bordeaux) and Pr Olivier Rascol (CHU Toulouse). This work was made possible by grants to V.P-F from the Association Française contre les Myopathies (AFM) and the Fondation pour la Recherche Médicale (FRM), to H.S from National Institutes of Health (GM089853) and to A.B by the program "Investissements d'avenir" ANR-10-IAIHU-06, 'The Programme Hospitalier de

For Peer Review

Recherche Clinique' (to I.L.B.) and the 7th framework program of the European Union (FP7, E12009DD, Neuromics). P.YWM is supported by a Clinician Scientist Fellowship Award (G1002570) from the Medical Research Council (UK).

REFERENCES

Amati-Bonneau P, Valentino M, Reynier P, Gallardo M, Bornstein B, Boissière A, et al. *OPA1* mutations induce mitochondrial DNA instability and optic atrophy 'plus' phenotype. Brain 2008; 131: 338-51.

An J, Shi J, He Q, Lui K, Liu Y, Huang Y, et al. CHM1/CHCHD6, a novel mitochondrial protein linked to regulation of mitofilin and mitochondrial cristae morphology. J Biol Chem 2012; 287: 7411-26.

Banci L, Bertini I, Ciofi-Baffoni S, Tokatlidis K. The coiled coil-helix coil-helix proteins may be redox proteins. FEBS Lett 2009; 583: 1699-702.

Banci L, Bertini I, Coffi-Baffoni S, Jaiswal D, Peruzzini R, Winkelman J. Structural characterization of CHCHD5 and CHCHD7: two atypical twin CX9C proteins. J Struct Biol 2012; 180: 190-200.

Bannwarth S, Figueroa A, Fragaki K, Destroismaisons L, Lacas-Gervais S, Lespinasse F, et al. The human *MSH5* (MutS Homolog 5) gene localizes to mitochondria and protects the mitochondrial genome from oxidative damage. Mitochondrion 2012; 12: 654-65.

Bradford M. A rapid and sensitive method for the quantitation of micrograms quantities of protein utilizing the principle of protein-dye binding. Annal Biochem 1976; 251: 69-72.

Brown TA, Tkachuk AN, Shtengel G, Kopek BG, Bogenhagen BF, Hess HF et al. Superresolution fluorescence imaging of mitochondrial nucleoids reveals their spatial range, limits and membrane interaction. Mol Cell Biol 2011; 31: 4494-5010.

Cavallo G. Genome-wide analysis of eukaryotic twin CX9C proteins. Mol Biosyst 2010; 6: 2459-70.

Chen H, Chan D. Physiological functions of mitochondrial fusion. Ann N Y Acad Sci 2010; 1201: 21-5.

Cogliati S, Frezza C, Soriano M, Varanita T, Quintana-Cabrera R, Corrado M, et al. Mitochondrial cristae shape determines respiratory chain supercomplexes and respiratory efficiency. Cell 2013; 155: 160-71.

Copeland W. Defects in mitochondrial DNA replication and human disease. Crit Rev Biochem Mol Biol 2012; 47: 64-74.

For Peer Review

Darshi M, Mendiola V, Mackey M, Murphy A, Koller A, Perkins G, et al. ChChd3, an inner mitochondrial membrane protein, is essential for maintening crista integrity and mitochondrial function. J Biol Chem 2011; 286: 2918-32.

Darshi M, Trinh K, Murphy A, Taylor S. Targeting and import mechanism of coiled-coil helix coiled-coil helix domain-containing protein 3 (ChChd3) into the mitochondrial intermembrane space. J Biol Chem 2012; 287: 39480-91.

DeJesus-Hernandez M, Mackenzie IR, Boeve BF, Boxer AL, Baker M, Rutherford NJ et al. Expanded GGGGCC hexanucleotide repeat in noncoding region of C9ORF72 causeschromosome 9p-linked FTD and ALS. Neuron 2011; 72: 245-56.

Delettre C, Laeners G, Griffoin J, Gigarel N, Lorenzo C, Belenguer P, et al. Nuclear gene *OPA1*, encoding a mitochondrial dynamin-related protein, is mutated in dominant optic atrophy. Nat Genet 2000; 26: 207-10.

Frezza C, Cipolat S, Martins de Brito O, Micaroni M, Beznoussenko G, Rudka T, et al. OPA1 controls apoptotic cristae remodeling independently from mitochondrial fusion. Cell 2006; 126: 177-89.

Hakonen A, Isohanni P, Paetau A, Herva R, Suomalainen A, Lonngvist T. Recessive Twinkle mutations in early onset encephalopathy with mtDNA depletion. Brain 2007; 130: 3032-40.

Hudson G, Amati-Bonneau P, Blakely E, Stewart J, He L, Schaefer A, et al. Mutation of *OPA1* causes dominant optic atrophy with external ophtalmoplegia, ataxia, deafness, and multiple mitochondrial DNA deletions: a novel disorder of mtDNA maintenance. Brain 2008; 131: 329-37.

Jans D, Wurm C, Riedel D, Wenzel D, Stagge F, Deckers M, et al. STED super-resolution microscopy reveals an array of MINOS clusters along human mitochondria. PNAS 2013; 110: 8936-41.

Karbowski M, Arnoult D, Chen H, Chan DC, Smith CL, Youle RJ. Quantitation of mitochondrial dynamics by photolabeling of individual organelles shows that mitochondrial fusion is blocked during the Bax activation phase of apoptosis. J Cell Biol. 2004;164: 493-9.

Kelley L, Sternberg M. Protein structure prediction on the web: a case study using the Phyre server. Nat Protoc 2009; 4: 363-71.

Kim JS, Xu X, Li H, Solomon D, Lane WS, Jin T, Waldman T. Mechanistic analysis of a DNA damage-induced, PTEN-dependent size checkpoint in human cells. Mol Cell Biol. 2011;31: 2756-71.

Koshiba T, Detmer S, Kaiser J, Chen H, McCaffery M, Chan D. Structural basis of mitochondrial tethering by mitofusin complexes. Science 2004; 305: 858-62.

Longen S, Bien M, Bihlmaier K, Kloeppel C, Kauff F, Hammermeister M, et al. Systematic analysis of the twin cx(9)c protein family. J Mol Biol 2009; 393: 356-68.

For Peer Review

Martherus RSRM, Sluiter W, Timmer EDJ, VanHerle SJV, Smeets HJM, Ayoubi TAY. Functional annotation of heart enriched mitochondrial genes GBAS and CHCHD10 through guilt by association. Bioch Biophys Res Com 2010; 402: 203-208.

Meeusen S, McCaffery M, Nunnari J. Mitochondrial fusion intermediates revealed *in vitro.* Science 2004; 305: 1747-52.

Moraes C, DiMauro S, Zeviani M, Lombes A, Shanske S, Miranda A, et al. Mitochondrial DNA deletions in progressive external ophtalmoplegia and Kearns-Sayre syndrome. N Engl J Med 1989; 18: 1293-9.

Naimi M, Bannwarth S, Procaccio V, Pouget J, Desnuelle C, Pellissier J, et al. Molecular analysis of *ANT1, TWINKLE* and *POLG* in patients with multiple deletions or depletion of mitochondrial DNA by dHPLC-based assay. Eur J Hum Genet 2006; 14: 917-22.

Paul R, Santucci S, Saunières S, Desnuelle C, Paquis-Flucklinger V. Rapid mapping of mitochondrial DNA deletions by large-fragment PCR. Trends Genet 1996; 12: 131-2.

Renton AE, Majounie E, Waite A, Simon-Sanchez J, Rollinson S, Gibbs JR et al. A hexanucleotide repeat expansion in C9ORF72 is the cause of chromosome 9p21-linked ALS-FTD. Neuron 2011; 72: 257-68.

Ronchi D, Garone C, Bordoni A, Rios PG, Calvo SE, Ripolone M et al. Next-generation sequencing reveals *DGUOK* mutations in adult patients with mtDNA deletions. Brain 2012; 135 : 3404-3415.

Rouzier C, Bannwarth S, Chaussenot A, Chevrollier A, Verschueren A, Bonello-Palot N, et al. The *MFN2* gene is responsible for mitochondrial DNA instability and optic atrophy 'plus' phenotype. Brain 2012; 135: 23-34.

Rouzier C, Le Guédard-Méreuze S, Fragaki K, Serre V, Miro J, Tuffery-Giraud S, et al. The severity of phenotype linked to *SUCLG1* mutations could be correlated with residual amount of SUCLG1 protein. J Med Genet 2010; 47: 670-6.

Rustin P, Chretien D, Bourgeron T, Gerard B, Rotig A, Saudubray J. Biochemical and molecular investigations in respiratory chain deficiencies. Clin Chem Acta 1994; 228: 31-51.

Schägger H, Pfeiffer K. The ratio of oxidative phosphorylation complexes I-IV in bovine heart mitochondria and the composition of respiratory chain supercomplexes. J Biol Chem 2001; 276: 37861-7.

Shapira A. Mitochondrial diseases. Lancet 2012; 379: 1825-34.

Smirnova E, Shurland D-L, Ryazantsev S, van der Blieck A. A human dynamin-related protein controls the distribution of mitochondria. J Cell Biol 2001; 143: 351-8.

Song Z, Ghochani M, McCaffery M, Frey T, Chan D. Mitofusins and OPA1 mediate sequential steps in mitochondrial membrane fusion. Mol Biol Cell 2009; 20: 3525-32.

For Peer Review

Stojanovski D, Bragozewski P, Chacinska A. The Mia pathway: A tight bond between protein transport and oxidative folding in mitochondria. BBA 2012; 1823: 1142-50.

Suomalainen A, Isohanni P. Mitochondrial DNA depletion syndromes-many genes, common mechanisms. Neuromuscul Disord 2010; 20: 429-37.

van der Laan M, Bohnert M, Wiedemann N, Pfanner N. Role of MINOS in mitochondrial membrane architecture and biogenesis. Trends Cell Biol 2012; 22: 185-92.

Wakabayashi J, Zhang Z, Wakabayashi N, Tamura Y, Fukaya M, Kensler TW, Iijima M, Sesaki H. The dynamin-related GTPase Drp1 is required for embryonic and brain development in mice. J Cell Biol 2009;186: 805-16.

Ylikallio E, Suomalainen A. Mechanisms of mitochondrial disease. Ann Med 2012; 44: 41-59.

Zanna C, Ghelli A, Porcelli A, Karbowski M, Youle R, Schimpf S, et al. *OPA1* mutations associated with dominant optic atrophy impair oxidative phosphorylation and mitochondrial fusion. Brain 2008; 131: 352-67.

Zick M, Rabl R, Reichert A. Cristae formation-linking ultrastructure and function of mitochondria. BBA 2009; 1793: 5-19.

Zuchner S, Mersiyanova I, Muglia M, Bissar-Tadmouri N, Rochelle J, Dadali E, et al. Mutations in the mitochondrial GTPase mitofusin 2 cause Charcot-Marie-Tooth neuropathy type 2A. Nat Genet 2004; 36: 459-1.

LEGENDS TO FIGURES

Figure 1. Pedigree of the first family. Solid symbols represent clinically affected individuals. * corresponds to individuals tested for segregation analysis.

Figure 2. Muscle analysis. A-B. Histopathology with Gomori modified trichrome (A) showing RRFs and COX/SDH stain (B) revealing COX-deficient fibres, which are recognized by the prevalent blue stain. **C.** Ultrastructure of skeletal muscle showing abnormal mitochondria with cristalloid inclusions (arrows) **D.** Blue native electrophoresis of muscle homogenates. Equal amounts (15 µg) of mitochondrial protein from age-matched control subjects (C) and patients IV-3 and V-2 were subjected to BN-PAGE, blotted onto a PVDF membrane and then incubated with specific antibodies. * corresponds to supplementary bands

For Peer Review

detected by anti-complex V antibody. **E.** Southern blot analysis revealing multiple deletion bands in addition to wild-type fragments in muscle of patients III-2, IV-11, IV-6 and V-2. C, control individual.

Figure 3. Mitochondrial fragmentation and ultrastructural alterations in skin fibroblasts. A. Cells obtained from a control (left panel) and patient V-10 (right panel) were analyzed by confocal microscopy using MitoTracker Red. Enlarged details of the areas are indicated. **B.** Mitochondrial phenotypes showed in A were quantified for 35 randomly-selected individual cells per each studied fibroblast cell line from 2 independent experiments. The data obtained were used to calculate the total length of the mitochondrial network per cell (left panel) and the average mitochondrial fragment length (right panel). Differences between the 2 cell lines were analyzed by Student's *t* test: significant (*: $0.05>p>0.01$), very significant (**: $0.01>p>0.001$) or extremely significant (***: $p<0.001$). **C-E.** Ultrastructural analysis of control (C) and patient V-10 (D-E) fibroblasts. Scale bar : 1µm **C.** Representative image of mitochondria with typical normal aspect found in control cells. **D.** Complete mitochondrial disorganization only found in patient cells. **E.** Moderate disorganization mainly found in patient cells.

Figure 4. Fusion analysis in patient fibroblasts. Control and patient fibroblasts expressing mitochondria-targeted photoactivatable GFP (mitoPAGFP) were stained with 7 nM tetramethylrhodamine ethyl ester (TMRE). mitoPAGFP was photoactivated with 405-nm laser in a small region of cells (30 x 30 pixels) at 0 min. Fibroblasts were observed with 15-min intervals for 60 min. Fluorescence intensity of mitoPAGFP was quantified using NIH Image J. Values represent the mean ± SME (n = 7 for control and 9 for patient).

Figure 5. Identification of the p.Ser59Leu mutation in *CHCHD10*. A. Schematic representation of the exome data analysis and data filtering. NS: non-synonymous variants; SS: splice site disrupting single nucleotide variants; I: exonic indels. Known variants

For Peer Review

correspond to SNPs and Indels already reported in dbSNP132, EVS (Exome Variant Server), HapMap, 1000 Genome databases and in-house control exomes. **B.** *CHCHD10* mutation sequences in patients III-2, IV-3, IV-6, IV-11, IV-13, IV-15, V-2, V-10 and a control (WT). **C.** Cross-species protein conservation of CHCHD10, flanking the altered amino acid p.Ser59. **D.** Model of CHCHD10 based on the CHCHD5 structure (PDB ID: 2LQL). Aliphatic, polar, basic and acidic residues are respectively in grey, black, blue and red. Disulfide bonds are in green. The polar residue Serine 59 is indicated with an asterisk.

Figure 6. Mitochondrial localization of CHCHD10. A. Expression of CHCHD10 protein in human tissues analyzed by western blotting using human multiple tissue blot. **B.** Colocalization of endogenous CHCHD10 protein with MitoTracker Red indicating mitochondrial localization for CHCHD10 in HeLa cells (overlay in yellow). **C.** Intact isolated mitochondria from HeLa cells (lanes 1-4) were incubated in presence (+) or in absence (-) of Proteinase K or Triton X-100 before analysis by immunoblotting using antibodies against CHCHD10, TOM20 (mitochondrial outer membrane protein) or SMAC (mitochondrial intermembrane space protein). To verify the purity of isolated mitochondria, total lysates (lane 5) and mitochondrial isolates (lane 6) were analyzed by immunoblotting using antibodies against CHCHD10, GAPDH (cytosolic protein) or PCNA (nuclear protein). **D.** Intact mitochondria were prepared and subjected to Na_2CO_3 extraction. A soluble protein fraction (S) and an integral membrane protein fraction (P) were prepared. Samples of an extract from intact mitochondria (input), and the fraction of each extraction were subjected to western blot analysis. VDAC and SMAC were used to identify behaviors of well defined mitochondrial proteins that are integral membrane protein and soluble, respectively. **E.** Isolated mitochondria from HeLa cells (lanes 1-2) were incubated in presence (+) or in absence (-) of Digitonin or Proteinase K before analysis by immunoblotting using antibodies against CHCHD10, MFN2 (outer membrane protein), mitofilin (inner membrane protein

For Peer Review

mainly facing the intermembrane space), SMAC (intermembrane space protein) or Hsp60 (mitochondrial matrix protein).

Figure 7. Submitochondrial localization of CHCHD10 using immunoelectron microscopy. A. Immunogold labeling of CHCHD10 in HeLa cells. Arrows point to the position of gold particles. Enlarged details of the areas are indicated by black boxes. Scale bar: 500nm. **B.** Localization of the gold particles as determined by immunogold labeling of CHCHD10 plotted on a scheme representing a part of a mitochondrion. OM, outer membrane; IM, inner membrane. The histogram shows the fraction of gold particules within the indicated distance to the cristae junction. The histogram and the graphical representation are based on the same measured gold particle localizations. **C**. Control immunogold labeling of Hsp60 in HeLa cells. Scale bar: 500nm. **D.** Localization of the gold particles as determined by immunogold labeling of Hsp60 plotted on a scheme representing a part of a mitochondrion. OM, outer membrane; IM, inner membrane. The histogram shows the fraction of gold particules within the indicated distance to the cristae junction. The histogram and the graphical representation are based on the same measured gold particle localizations.

Figure 8. Effects of overexpression of wild-type and pathogenic CHCHD10 alleles on mitochondrial network in HeLa cells. Transfections were performed with empty vector (EV) or vectors encoding either wild-type CHCHD10-Flag (WT) or mutant CHCHD10-Flag (S59L). **A.** Western blot on HeLa cells extracts using antibodies against Flag, CHCHD10 or β-tubulin. NS, non specific. **B.** Analysis of DAPI (blue), Mitotracker (red) staining and CHCHD10 (green) immuno-labeling by fluorescence microscopy in HeLa cells transfected with either wild-type CHCHD10-Flag (WT) or mutant CHCHD10-Flag (S59L). **C.** Quantification of mitochondrial phenotypes of cells transfected with empty vector (EV) or vectors encoding either wild-type CHCHD10-Flag (WT) or mutant CHCHD10-Flag (S59L). Thirty five randomly-selected individual cells per each transfection were analyzed from 2

For Peer Review

independent experiments. The data obtained were used to calculate the total length of the mitochondrial network per cell. Differences between the 2 cell lines were analyzed by Student's *t* test: very significant (**: 0.01>*p*>0.001) or extremely significant (***: *p*<0.001).

Figure 9. Effects of overexpression of wild-type and pathogenic CHCHD10 alleles on cristae morphology in HeLa cells. A. Representative image of mitochondria after transfection with the empty vector. **B**. Representative image of mitochondria in cells overexpressing the wild-type CHCHD10 allele. **C-D.** Representative images of mitochondria in cells overexpressing the mutant CHCHD10 allele (S59L).

Table 1. Clinical data of affected members. M, male ; F, female ; AO, Age at onset ; AB, age at biopsy ; AD, age of death ; †, deceased; ?, unknown ; m, muscle; MND, motor neuron disease ; RRF, ragged-red fibers; COX-, COX negative fibers ; ↓, decreased; +, present; -, absent.

Table 2. Respiratory chain analysis in patient fibroblasts A-B. Spectrophotometric analysis of the respiratory chain enzyme activities in patient fibroblasts in glucose (A) and in galactose medium (B). CS, citrate synthase. Results are expressed as extreme absolute values or absolute values for controls or patients, respectively. Values are expressed in nanomols of substrate per minute per milligram of proteins (lowered values are in grey). **C-D.** Polarographic analysis of the respiratory chain in patient fibroblasts in glucose (C) and in galactose medium (D). G3P, glycerol 3-phosphate. Results are expressed as extreme absolute values or absolute values for controls or patients, respectively. Values are expressed in nanomols of oxygen per minute per milligram of proteins (lowered values are in grey).

For Peer Review